

A separation-of-variable dynamic stiffness matrix method for the free vibration of orthotropic rectangular thin plates

Shiyi Mei^a, Colin Caprani^{a,*}, Daniel Cantero^b

^a*Department of Civil Engineering, Monash University, Melbourne, Victoria, Australia*

^b*Department of Structural Engineering, Norwegian University of Science & Technology
NTNU, Trondheim, Norway*

Abstract

A separation-of-variable dynamic stiffness matrix (SOV-DSM) method is proposed for the free vibration analysis of an orthotropic rectangular thin plate with general homogeneous boundary conditions. Firstly, the exact SOV solution satisfying Rayleigh's principle is extended to handle arbitrary boundary conditions and then applied to develop closed-form dynamic stiffness formulations. Then, an enhanced Wittrick–Williams (W-W) algorithm is used to solve the eigenvalue problem rather than solving the highly nonlinear eigenvalue equations. The J_0 count problem involved in applying the W-W algorithm is addressed by providing an explicit and closed-form expression for the J_0 term based on the characteristics of the SOV solution. Furthermore, a numerical technique is provided to calculate the mode shape of the plate with any arbitrary boundary conditions. The accuracy of the proposed method is validated through numerical experiments by comparison with other analytical solutions.

*Corresponding author

Email addresses: shiyi.mei1@monash.edu (Shiyi Mei), colin.caprani@monash.edu (Colin Caprani), daniel.cantero@ntnu.no (Daniel Cantero)

1 1. Introduction

2 Rectangular plates play an important role in various engineering fields,
3 including civil, mechanical, and aerospace engineering [1]. The free vibration
4 of plates has been a fundamental research problem for over two centuries.
5 The earliest exact solutions for this problem are the Navier [2] and Levy
6 [3] solutions, which require at least one pair of opposite edges to be simply
7 supported or guided. To solve problems with other boundary conditions,
8 approximate solutions such as the Rayleigh–Ritz method [4–8], the Galerkin
9 method [9–13] and finite element method (FEM) [14–18] have been widely
10 applied. For most approximation methods, beam functions [19–22], polyno-
11 mials [23–27], trigonometric functions [28–32], and their combinations [33–
12 37] are commonly used as the assumed approximate functions. The accuracy
13 of these solutions depends on how well the assumed approximate functions
14 represent the displacement of the plate.

15 Besides the approximation methods, several analytical methods have been
16 developed over past decades, including the Kantorovich-Krylov method [38–
17 44], the symplectic method [45–50], the separation-of-variable (SOV) method
18 [46, 51–59], the dynamic stiffness matrix (DSM) method [60–71], and series
19 expansion-based methods [72–90]. The series expansion-based methods in-
20 clude the superposition method [72–77], Fourier series method [78–82], the
21 finite integral transform method [83–87], and other series methods [88–90].
22 These methods represent the plate displacement in terms of an infinite se-
23 ries and mostly are capable of handling any general boundary conditions.
24 However, sufficient truncation of the series is required to ensure the accuracy
25 and convergence of the results, and the eigenvalue equation is generally dif-
26 ficult to express explicitly. Therefore, solving the corresponding eigenvalue
27 problem can be computationally expensive.

28 Despite being a powerful method for the dynamic analysis of plate as-
29 semblies, the FEM requires a sufficient number of elements and is compu-
30 tationally expensive to accurately capture higher-order modes. Thus, the

31 DSM method was developed as an accurate and efficient analytical approach
32 to alternatively solve complex plate structures [63, 64]. The DSM can be
33 considered as an analytical FEM since the mode functions of the plate are
34 expressed by analytical solutions, where Levy-type solution [65] or compo-
35 nents of Fourier series [66–70] are applied. To avoid solving the cumbersome
36 transcendental frequency equation directly, the Wittrick-Williams (W-W)
37 algorithm [91] is applied to the eigenvalue problem. The W-W algorithm
38 determines the lower and upper bounds of natural frequencies to arbitrary
39 precision rather than solving the frequency equation directly. Thus, the DSM
40 has the potential to be effectively and systematically solved using the W-W
41 algorithm. However, a critical part in applying the W-W algorithm is to
42 determine all natural frequencies of the fully clamped structure within the
43 interested frequency range, *a priori*. Strategies such as using a sufficiently
44 fine mesh or including a sufficient number of terms in series expansions [67]
45 can ensure that all fully clamped frequencies are accounted for, thereby main-
46 taining the accuracy of the algorithm. However, these approaches are compu-
47 tionally expensive and complex, posing a significant obstacle to the wider
48 adoption and application of the DSM method based on the W-W algorithm
49 [92, 93]. To resolve the fully clamped plate problem, Liu and Banerjee [71]
50 suggested that the frequencies can be indirectly obtained from the simply
51 supported plate problem, where the Navier solution serves as the analytical
52 solution. This idea provides a significant enhancement to the W-W algo-
53 rithm, increasing the efficiency of applying DSM methods [69, 70]. However,
54 most solutions applied in these DSM methods are not explicit and closed-
55 form, but are expressed in an infinite series form, where a sufficient number
56 of truncation terms might be required to ensure accuracy.

57 Inspired by the Navier and Levy solutions, Xing and Liu [51] proposed
58 the SOV method, which provides concise and explicit eigensolutions. The
59 mode shape function has a separable form, $\phi(x)\psi(y)$, requiring only one $\phi(x)$
60 and one $\psi(y)$ for each mode order, allowing each eigenvalue equation to be

61 explicitly expressed. However, this SOV method is not suitable to deal with
62 plates with free boundary conditions. Therefore, an extended SOV method
63 [52, 53] based on the Rayleigh quotient was proposed to accommodate plates
64 with all four classical boundary conditions, i.e., simply supported, clamped,
65 guided, and free. Based on the Rayleigh quotient model, alternative iterative
66 and improved SOV methods have been subsequently proposed [54]. Although
67 SOV methods provide concise closed-form analytical solutions, they require
68 solving a specific set of highly nonlinear eigenvalue equations for each type
69 of boundary condition. However, even when considering only the four classic
70 homogeneous cases, it becomes evident that 55 different boundary condition
71 combinations exist for a rectangular plate, making the process tedious.

72 In this study, a separation-of-variable dynamic stiffness matrix (SOV-
73 DSM) method is proposed to avoid solving transcendental eigenvalue equa-
74 tions in SOV methods. It also fills the gap caused by the limitation of
75 closed-form dynamic stiffness formulations available for existing plate struc-
76 tures. Firstly, the SOV method is further extended to analyze the vibra-
77 tions of plates with elastically restrained edges based on Rayleigh's principle.
78 This extended SOV solution is then employed to construct dynamic stiffness
79 matrices that accommodate general homogeneous boundary conditions. By
80 taking advantage of both the SOV and DSM methods, an enhanced W-W
81 algorithm is developed to solve the eigenvalue problem without directly solv-
82 ing the eigenvalue equations. This enhanced approach resolves the challenge
83 of determining fully clamped frequencies, also called the J_0 count problem, a
84 well-known limitation in the application of the W-W algorithm. Two types
85 of explicit and closed-form expressions for the J_0 term, based on specific sup-
86 ports such as simply supported, guided, or their combinations, are provided
87 to improve the computational efficiency of the eigenvalue problem. In ad-
88 dition, a novel numerical technique is proposed to compute the mode shape
89 coefficients.

90 The paper is structured as follows: Section 2 presents the SOV-DSM

91 formulations derived from the extended SOV method, which accommodates
 92 elastically restrained boundary conditions. In Section 3, an enhanced W-
 93 W algorithm that resolves the J_0 count problem is provided to solve the
 94 dynamic stiffness matrices. The explicit and closed-form expression for the
 95 J_0 term is provided. In addition, a novel numerical technique is proposed to
 96 compute the mode shape of the plate with arbitrary boundary conditions.
 97 Section 4 validates the proposed method through numerical experiments by
 98 comparison under several boundary conditions. Finally, the conclusions of
 99 this paper are presented in Section 5.

100 **2. Separation-of-variable dynamic stiffness matrix formulation**

101 In this section, the SOV-DSM formulations for the free vibration analysis
 102 of orthotropic rectangular thin plates are developed. Section 2.1 presents the
 103 mathematical model of the extended separation-of-variable method. Then,
 104 the SOV-DSM formulations in the x - and y -directions will be proposed sep-
 105 arately in Section 2.2 and Section 2.3, according to the boundary conditions
 106 of the plate.

107 *2.1. Mathematical model for separation-of-variable method*

108 Consider a thin orthotropic rectangular plate of length $2a$ and width
 109 $2b$, with all four edges restrained by vertical translational springs k^v and
 110 rotational springs k^r , as shown in Figure 1. The coordinate origin is located
 111 at the center of the plate.

112 The governing differential equation for the free vibration of a thin or-
 113 thotropic plate is given by [54]:

$$D_{11} \frac{\partial^4 w}{\partial \xi^4} + 2D_3 \chi^2 \frac{\partial^4 w}{\partial \xi^2 \partial \eta^2} + D_{22} \chi^4 \frac{\partial^4 w}{\partial \eta^4} = \rho h a^4 \omega^2 w, \quad (1)$$

114 where $\chi = a/b$ is the aspect ratio; $\xi = x/a$ and $\eta = y/b$ are the normalized

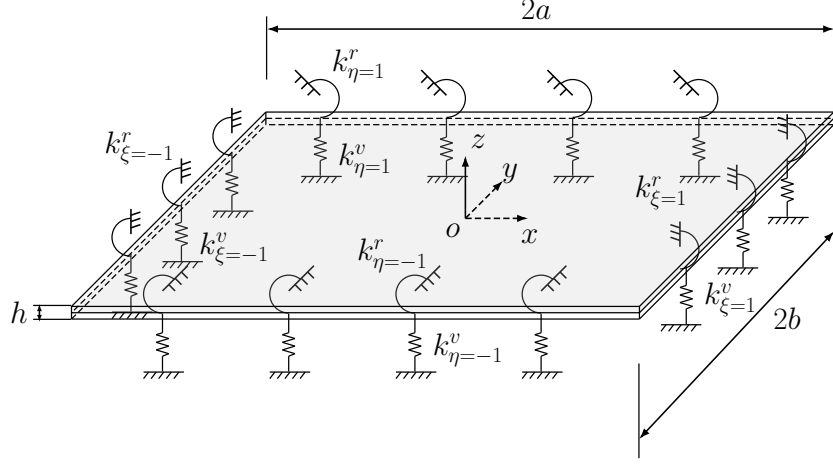


Figure 1: The orthotropic rectangular plate with all edges elastically restrained.

¹¹⁵ coordinates, and the bending stiffness parameters are defined as:

$$\begin{aligned} D_{11} &= \frac{E_1 h^3}{12(1 - v_{12}v_{21})}, & D_{22} &= \frac{E_2 h^3}{12(1 - v_{12}v_{21})}, \\ D_{66} &= \frac{G_{12} h^3}{12}, & D_{12} &= v_{12} D_{22} = v_{21} D_{11}, & D_3 &= D_{12} + 2D_{66}, \end{aligned} \quad (2)$$

¹¹⁶ where ρ and h denote the mass density and thickness of the plate, respectively;
¹¹⁷ E_1 and E_2 are the Young's moduli in the x - and y -directions, respectively;
¹¹⁸ G_{12} is the shear modulus, and v_{12} and v_{21} are the Poisson's ratios.

¹¹⁹ Instead of solving the free vibration of the thin orthotropic plate using
¹²⁰ Equation (1), it is suggested that the vibration of the thin plate can also be
¹²¹ solved using the Rayleigh quotient variational principle [52]:

$$\delta U = \delta T, \quad (3)$$

¹²² where δ denotes variation, U is the magnitude of the potential energy of the
¹²³ plate, and T represents the magnitude of the kinetic energy of the plate. The

¹²⁴ potential energy of the plate can be expressed as [53]:

$$U^I = \frac{1}{2} \iint \left[D_{11} \left(\frac{\partial^2 W}{\partial x^2} \right)^2 + 2D_{12} \frac{\partial^2 W}{\partial x^2} \frac{\partial^2 W}{\partial y^2} + D_{22} \left(\frac{\partial^2 W}{\partial y^2} \right)^2 + 4D_{66} \left(\frac{\partial^2 W}{\partial x \partial y} \right)^2 \right] dx dy. \quad (4)$$

¹²⁵ And the kinetic energy is:

$$T = \frac{1}{2} \iint \rho h \left(\frac{\partial W}{\partial t} \right)^2 dx dy. \quad (5)$$

¹²⁶ Assuming the solution of the deflection $W(x, y; t) = w(x, y)e^{i\omega t}$ for har-
¹²⁷ monic plate motion, where $i = \sqrt{-1}$, $w(x, y)$ is the mode shape, and ω is the
¹²⁸ radial frequency. By substituting $W(x, y; t) = w(x, y)e^{i\omega t}$ into Equations (4)
¹²⁹ and (5) and expressing the system in dimensionless coordinates, we have:

$$U^I = \frac{ab}{2} \iint \left[\frac{D_{11}}{a^4} \left(\frac{\partial^2 w}{\partial \xi^2} \right)^2 + \frac{2D_{12}}{a^2 b^2} \frac{\partial^2 w}{\partial \xi^2} \frac{\partial^2 w}{\partial \eta^2} + \frac{D_{22}}{b^4} \left(\frac{\partial^2 w}{\partial \eta^2} \right)^2 + \frac{4D_{66}}{a^2 b^2} \left(\frac{\partial^2 w}{\partial \xi \partial \eta} \right)^2 \right] d\xi d\eta, \quad (6)$$

¹³⁰ and

$$T = \omega^2 \frac{ab}{2} \rho h \iint w^2 d\xi d\eta = \omega^2 T_0, \quad (7)$$

¹³¹ where, T_0 is defined as the coefficient of the kinetic energy.

¹³² The separable form of the mode shape function $w(\xi, \eta)$ is given by:

$$w(\xi, \eta) = \phi(\xi)\psi(\eta), \quad (8)$$

¹³³ where $\phi(\xi)$ and $\psi(\eta)$ can be expressed as:

$$\phi(\xi) = A_1 \sin(\alpha_1 \xi) + A_2 \cos(\alpha_1 \xi) + A_3 \sinh(\beta_1 \xi) + A_4 \cosh(\beta_1 \xi), \quad (9a)$$

$$\psi(\eta) = B_1 \sin(\alpha_2 \eta) + B_2 \cos(\alpha_2 \eta) + B_3 \sinh(\beta_2 \eta) + B_4 \cosh(\beta_2 \eta). \quad (9b)$$

¹³⁴ Based on Equation (3), the frequencies ω_x and ω_y , corresponding to the
¹³⁵ mode shapes $\phi(\xi)$ and $\psi(\eta)$, respectively, are assumed to be independent of
¹³⁶ each other. This is a common and important assumption in SOV methods,
¹³⁷ and ω_x and ω_y can be different in a mathematical sense [53].

¹³⁸ *2.2. Dynamic stiffness matrix corresponding to ω_x*

¹³⁹ For given general homogeneous boundary conditions, we can first assume
¹⁴⁰ that the mode shape $\psi(\eta)$ corresponding to the y -direction is known. Sup-
¹⁴¹ posing the edges of the plate in both the x - and y -directions are elastically
¹⁴² restrained by homogeneous vertical translational and rotational springs. The
¹⁴³ vertical translational and rotational springs at the $\xi = -1$ end are denoted
¹⁴⁴ as $k_{\xi=-1}^v$ and $k_{\xi=-1}^r$, respectively, and at the $\xi = 1$ end as $k_{\xi=1}^v$ and $k_{\xi=1}^r$,
¹⁴⁵ respectively. Thus, the potential energy along the supported edge in the
¹⁴⁶ x -direction can be expressed by:

$$U^x = \int \left[k_{\xi=-1}^r \left(\frac{\partial W}{\partial x} \right)^2 + k_{\xi=-1}^v (W)^2 \right]_{x=-a} dy + \int \left[k_{\xi=1}^r \left(\frac{\partial W}{\partial x} \right)^2 + k_{\xi=1}^v (W)^2 \right]_{x=a} dy. \quad (10)$$

¹⁴⁷ From Equation (10), the magnitude of potential energy along the plate edges
¹⁴⁸ in the x -direction, expressed in dimensionless coordinates, is obtained as:

$$U^x = ab \int \left[\frac{k_{\xi=-1}^r}{a^3} \left(\frac{\partial w}{\partial \xi} \right)^2 + \frac{k_{\xi=-1}^v}{a} (w)^2 \right]_{\xi=-1} d\eta \\ + ab \int \left[\frac{k_{\xi=1}^r}{a^3} \left(\frac{\partial w}{\partial \xi} \right)^2 + \frac{k_{\xi=1}^v}{a} (w)^2 \right]_{\xi=1} d\eta. \quad (11)$$

¹⁴⁹ The magnitude of total potential energy of the plate in the x -direction can
¹⁵⁰ be obtained from Equations (6) and (11) as:

$$U = U^I + U^x \\ = \frac{ab}{2} \iint \left[\frac{D_{11}}{a^4} \left(\frac{\partial^2 w}{\partial \xi^2} \right)^2 + \frac{2D_{12}}{a^2 b^2} \frac{\partial^2 w}{\partial \xi^2} \frac{\partial^2 w}{\partial \eta^2} + \frac{D_{22}}{b^4} \left(\frac{\partial^2 w}{\partial \eta^2} \right)^2 \right. \\ \left. + \frac{4D_{66}}{a^2 b^2} \left(\frac{\partial^2 w}{\partial \xi \partial \eta} \right)^2 \right] d\xi d\eta \\ + ab \int \left[\frac{k_{\xi=1}^r}{a^3} \left(\frac{\partial w}{\partial \xi} \right)^2 + \frac{k_{\xi=1}^v}{a} (w)^2 \right]_{\xi=1} d\eta \\ + ab \int \left[\frac{k_{\xi=-1}^r}{a^3} \left(\frac{\partial w}{\partial \xi} \right)^2 + \frac{k_{\xi=-1}^v}{a} (w)^2 \right]_{\xi=-1} d\eta \quad (12)$$

¹⁵¹ By substituting Equation (8) into Equation (12), we have:

$$\begin{aligned}
U = & \frac{ab}{2} \int_{-1}^1 \left[\frac{D_{11}}{a^4} I_1 \left(\frac{d^2 \phi}{d\xi^2} \right)^2 + \frac{2D_{12}}{a^2 b^2} I_2 \frac{d^2 \phi}{d\xi^2} \phi + \frac{D_{22}}{b^4} I_4 \phi^2 \right. \\
& \left. + \frac{4D_{66}}{a^2 b^2} I_3 \left(\frac{d\phi}{d\xi} \right)^2 \right] d\xi \\
& + ab I_1 \left[\frac{k_{\xi=-1}^r}{a^3} \left(\frac{d\phi}{d\xi} \right)^2 + \frac{k_{\xi=-1}^v}{a} (\phi)^2 \right]_{\xi=-1} \\
& + ab I_1 \left[\frac{k_{\xi=1}^r}{a^3} \left(\frac{d\phi}{d\xi} \right)^2 + \frac{k_{\xi=1}^v}{a} (\phi)^2 \right]_{\xi=1},
\end{aligned} \tag{13}$$

¹⁵² where the integral parameters I_1 , I_2 , I_3 , and I_4 are defined and expressed in
¹⁵³ Appendix A.

¹⁵⁴ By taking Equation (8) into account, the coefficient T_0 of the kinetic
¹⁵⁵ energy from Equation (7) for the plate in the x -direction can be expressed
¹⁵⁶ as:

$$T_0 = \frac{ab}{2} \rho h \iint w^2 d\xi d\eta = \frac{ab}{2} \rho h I_1 \int_{-1}^1 \phi^2 d\xi. \tag{14}$$

¹⁵⁷ Taking the Rayleigh principle in the form:

$$\delta U = \omega_x^2 \delta T_0, \tag{15}$$

¹⁵⁸ and by substituting Equations (13) and (14) into Equation (15), and relieving

¹⁵⁹ $\delta\phi$ and $\delta\frac{d\phi}{d\xi}$ in Equation (15) by calculus of variations, yields:

$$\begin{aligned}
 0 = & \int_{-1}^1 \left[\frac{D_{11}}{a^4} I_1 \frac{d^4\phi}{d\xi^4} + \left(\frac{2D_{12}}{a^2 b^2} I_2 - \frac{4D_{66}}{a^2 b^2} I_3 \right) \frac{d^2\phi}{d\xi^2} \right. \\
 & + \left. \left(\frac{D_{22}}{b^4} I_4 - \omega_x^2 \rho h I_1 \right) \phi \right] \delta\phi d\xi \\
 & + \frac{2k_{\xi=-1}^v}{a} I_1 (\phi \delta\phi)_{\xi=-1} + \frac{2k_{\xi=1}^v}{a} I_1 (\phi \delta\phi)_{\xi=1} \\
 & + \left[\left(\frac{4D_{66}}{a^2 b^2} I_3 - \frac{D_{12}}{a^2 b^2} I_2 \right) \frac{d\phi}{d\xi} - \frac{D_{11}}{a^4} I_1 \frac{d^3\phi}{d\xi^3} \right] \delta\phi \Big|_{\xi=-1}^{\xi=1} \\
 & + \left(\frac{D_{12}}{a^2 b^2} I_2 \phi + \frac{D_{11}}{a^4} I_1 \frac{d^2\phi}{d\xi^2} \right) \delta \frac{d\phi}{d\xi} \Big|_{\xi=-1}^{\xi=1} \\
 & + \frac{2k_{\xi=-1}^r}{a^3} I_1 \left(\frac{d\phi}{d\xi} \delta \frac{d\phi}{d\xi} \right)_{\xi=-1} + \frac{2k_{\xi=1}^r}{a^3} I_1 \left(\frac{d\phi}{d\xi} \delta \frac{d\phi}{d\xi} \right)_{\xi=1}.
 \end{aligned} \tag{16}$$

¹⁶⁰ Thus, the governing differential equation in the x -direction can be obtained
¹⁶¹ from the integration part in Equation (16):

$$\frac{d^4\phi}{d\xi^4} + 2\chi^2 \left(\frac{D_{12}I_2}{D_{11}I_1} - 2\frac{D_{66}I_3}{D_{11}I_1} \right) \frac{d^2\phi}{d\xi^2} + \left(\chi^4 \frac{D_{22}I_4}{D_{11}I_1} - a^4 \Omega_x^4 \right) \phi = 0, \tag{17}$$

¹⁶² where $\Omega_x = \sqrt[4]{\omega_x^2 \rho h / D_{11}}$. By substituting $\phi(\xi) = A e^{\mu\xi}$ into Equation (17),
¹⁶³ we obtain:

$$\mu^4 + 2\chi^2 \left(\frac{D_{12}I_2}{D_{11}I_1} - 2\frac{D_{66}I_3}{D_{11}I_1} \right) \mu^2 + \left(\chi^4 \frac{D_{22}I_4}{D_{11}I_1} - a^4 \Omega_x^4 \right) = 0. \tag{18}$$

¹⁶⁴ And so the solution for μ can be expressed as:

$$\mu_{1,2} = \pm i\alpha_1, \quad \mu_{3,4} = \pm \beta_1, \tag{19}$$

¹⁶⁵ where,

$$\alpha_1 = \chi \sqrt{\left(\frac{D_{12}I_2}{D_{11}I_1} - 2\frac{D_{66}I_3}{D_{11}I_1} \right)^2 - \frac{D_{22}I_4}{D_{11}I_1} + b^4\Omega_x^4 + \frac{D_{12}I_2}{D_{11}I_1} - 2\frac{D_{66}I_3}{D_{11}I_1}}, \quad (20a)$$

$$\beta_1 = \chi \sqrt{\left(\frac{D_{12}I_2}{D_{11}I_1} - 2\frac{D_{66}I_3}{D_{11}I_1} \right)^2 - \frac{D_{22}I_4}{D_{11}I_1} + b^4\Omega_x^4 - \frac{D_{12}I_2}{D_{11}I_1} + 2\frac{D_{66}I_3}{D_{11}I_1}}. \quad (20b)$$

¹⁶⁶ The boundary conditions along the edges in the x -direction can be obtained
¹⁶⁷ from the remaining $\delta\phi$ and $\delta\frac{d\phi}{d\xi}$ parts in Equation (16). The shear force
¹⁶⁸ equilibrium can be obtained from the $\delta\phi$ part:

$$\begin{aligned} & \left[\left(\frac{4D_{66}}{a^2b^2}I_3 - \frac{D_{12}}{a^2b^2}I_2 \right) \frac{d\phi}{d\xi} - \frac{D_{11}}{a^4}I_1 \frac{d^3\phi}{d\xi^3} \right] \Big|_{\xi=-1}^{\xi=1} \\ & + \frac{2k_{\xi=-1}^v}{a} I_1(\phi)_{\xi=-1} + \frac{2k_{\xi=1}^v}{a} I_1(\phi)_{\xi=1} = 0, \end{aligned} \quad (21)$$

¹⁶⁹ and from the $\delta\frac{d\phi}{d\xi}$ part, the bending moment equilibrium:

$$\begin{aligned} & \left(\frac{D_{12}}{a^2b^2}I_2\phi + \frac{D_{11}}{a^4}I_1 \frac{\partial^2\phi}{\partial\xi^2} \right) \Big|_{\xi=-1}^{\xi=1} \\ & + \frac{2k_{\xi=-1}^r}{a^3} I_1 \left(\frac{\partial\phi}{\partial\xi} \right)_{\xi=-1} + \frac{2k_{\xi=1}^r}{a^3} I_1 \left(\frac{\partial\phi}{\partial\xi} \right)_{\xi=1} = 0. \end{aligned} \quad (22)$$

¹⁷⁰ Thus, we can obtain the shear force and bending moment equilibrium along

¹⁷¹ the edges $\xi = -1$ and $\xi = 1$ from Equations (21) and (22), respectively, as:

$$\frac{d^3\phi}{d\xi^3} - \chi^2 \left(\frac{4D_{66}I_3}{D_{11}I_1} - \frac{D_{12}I_2}{D_{11}I_1} \right) \frac{d\phi}{d\xi} + \frac{2a^3k_{\xi=-1}^v}{D_{11}}\phi = 0, \quad \xi = -1, \quad (23a)$$

$$\frac{d^2\phi}{d\xi^2} + \frac{\chi^2 D_{12}I_2}{D_{11}I_1}\phi - \frac{2ak_{\xi=-1}^r}{D_{11}}\frac{d\phi}{d\xi} = 0, \quad \xi = -1, \quad (23b)$$

$$\frac{d^3\phi}{d\xi^3} - \chi^2 \left(\frac{4D_{66}I_3}{D_{11}I_1} - \frac{D_{12}I_2}{D_{11}I_1} \right) \frac{d\phi}{d\xi} - \frac{2a^3k_{\xi=1}^v}{D_{11}}\phi = 0, \quad \xi = 1, \quad (23c)$$

$$\frac{d^2\phi}{d\xi^2} + \frac{\chi^2 D_{12}I_2}{D_{11}I_1}\phi + \frac{2ak_{\xi=1}^r}{D_{11}}\frac{d\phi}{d\xi} = 0, \quad \xi = 1. \quad (23d)$$

¹⁷² Substituting Equation (9a) into Equation (23), and denoting $k_\xi^{v*} \equiv \frac{2a^3k_\xi^v}{D_{11}}$,
¹⁷³ $k_\eta^{r*} \equiv \frac{2ak_\xi^r}{D_{11}}$, $S_{\alpha_1} \equiv \sin \alpha_1$, $C_{\alpha_1} \equiv \cos \alpha_1$, $Sh_{\beta_1} \equiv \sinh \beta_1$, and $Ch_{\beta_1} \equiv \cosh \beta_1$,
¹⁷⁴ we have:

$$\begin{bmatrix} \gamma_1 C_{\alpha_1} - k_{\xi=-1}^{v*} S_{\alpha_1} & \gamma_1 S_{\alpha_1} + k_{\xi=-1}^{v*} C_{\alpha_1} & \gamma_2 Ch_{\beta_1} - k_{\xi=-1}^{v*} Sh_{\beta_1} \\ \gamma_3 S_{\alpha_1} + k_{\xi=-1}^{r*} \alpha_1 C_{\alpha_1} & -\gamma_3 C_{\alpha_1} + k_{\xi=-1}^{r*} \alpha_1 S_{\alpha_1} & \gamma_4 Sh_{\beta_1} + k_{\xi=-1}^{r*} \beta_1 Ch_{\beta_1} \\ -\gamma_1 C_{\alpha_1} + k_{\xi=1}^{v*} S_{\alpha_1} & \gamma_1 S_{\alpha_1} + k_{\xi=1}^{v*} C_{\alpha_1} & -\gamma_2 Ch_{\beta_1} + k_{\xi=1}^{v*} Sh_{\beta_1} \\ \gamma_3 S_{\alpha_1} + k_{\xi=1}^{r*} \alpha_1 C_{\alpha_1} & \gamma_3 C_{\alpha_1} - k_{\xi=1}^{r*} \alpha_1 S_{\alpha_1} & \gamma_4 Sh_{\beta_1} + k_{\xi=1}^{r*} \beta_1 Ch_{\beta_1} \\ -\gamma_2 Sh_{\beta_1} + k_{\xi=-1}^{v*} Ch_{\beta_1} & -\gamma_4 Ch_{\beta_1} - k_{\xi=-1}^{r*} \beta_1 Sh_{\beta_1} & \\ -\gamma_2 Sh_{\beta_1} + k_{\xi=1}^{v*} Ch_{\beta_1} & \gamma_4 Ch_{\beta_1} + k_{\xi=1}^{r*} \beta_1 Sh_{\beta_1} & \end{bmatrix} \begin{Bmatrix} A_1 \\ A_2 \\ A_3 \\ A_4 \end{Bmatrix} = \begin{Bmatrix} 0 \\ 0 \\ 0 \\ 0 \end{Bmatrix}, \quad (24)$$

¹⁷⁵ or,

$$\mathbf{R}_x \mathbf{A} = \mathbf{0}, \quad (25)$$

¹⁷⁶ where,

$$\begin{aligned}\gamma_1 &= -\alpha_1^3 - \chi^2 \left(\frac{4D_{66}S_3}{D_{11}I_1} - \frac{D_{12}I_2}{D_{11}I_1} \right) \alpha_1, \\ \gamma_2 &= \beta_1^3 - \chi^2 \left(\frac{4D_{66}S_3}{D_{11}I_1} - \frac{D_{12}I_2}{D_{11}I_1} \right) \beta_1, \\ \gamma_3 &= -\alpha_1^2 + \frac{\chi^2 D_{12}I_2}{D_{11}I_1}, \\ \gamma_4 &= \beta_1^2 + \frac{\chi^2 D_{12}I_2}{D_{11}I_1}.\end{aligned}\tag{26}$$

¹⁷⁷ Note that the classic boundary conditions can be obtained by selecting ex-
¹⁷⁸ tremely large or small spring stiffness constants. For non-trivial solutions,
¹⁷⁹ the characteristic equation or eigenvalue equation is obtained from the de-
¹⁸⁰ terminant of the matrix \mathbf{R}_x in Equation (25), which must be zero. However,
¹⁸¹ solving these transcendental equations is cumbersome and so the DSM is
¹⁸² introduced to avoid such a computation.

¹⁸³ To develop the plate's dynamic stiffness matrix, with the help of Equa-
¹⁸⁴ tion (9a), the vertical displacement and rotation corresponding to the mode
¹⁸⁵ shape $\phi(\xi)$ along the x -direction at edges $\xi = -1$ and $\xi = 1$ can be expressed
¹⁸⁶ as:

$$\begin{Bmatrix} \phi_{\xi=-1} \\ \frac{d\phi}{d\xi}_{\xi=-1} \\ \phi_{\xi=1} \\ \frac{d\phi}{d\xi}_{\xi=1} \end{Bmatrix} = \begin{bmatrix} -S_{\alpha_1} & C_{\alpha_1} & -Sh_{\beta_1} & Ch_{\beta_1} \\ \alpha_1 C_{\alpha_1}/a & \alpha_1 S_{\alpha_1}/a & \beta_1 Ch_{\beta_1}/a & -\beta_1 Sh_{\beta_1}/a \\ S_{\alpha_1} & C_{\alpha_1} & Sh_{\beta_1} & Ch_{\beta_1} \\ \alpha_1 C_{\alpha_1}/a & -\alpha_1 S_{\alpha_1}/a & \beta_1 Ch_{\beta_1}/a & \beta_1 Sh_{\beta_1}/a \end{bmatrix} \begin{Bmatrix} A_1 \\ A_2 \\ A_3 \\ A_4 \end{Bmatrix}, \tag{27}$$

¹⁸⁷ or,

$$\delta_x = \mathbf{Q}_x \mathbf{A}. \tag{28}$$

¹⁸⁸ Solving for the eigenvector \mathbf{A} , and then substituting into Equation (25), we
¹⁸⁹ obtain:

$$\mathbf{R}_x \mathbf{A} = \mathbf{R}_x \mathbf{Q}_x^{-1} \delta_x = \mathbf{0}. \tag{29}$$

190 where the dynamic stiffness matrix, denoted as $\mathbf{K}_x = \mathbf{R}_x \mathbf{Q}_x^{-1}$, can be ob-
 191 tained from Equation (29). This matrix can be used to compute the natural
 192 frequencies of the system instead of solving the eigenvalue equation, and the
 193 method for the computation will be given in Section 3.

194 *2.3. Dynamic stiffness matrix corresponding to ω_y*

195 In this section, the mode shape $\phi(\xi)$ derived in *Section 2.2* is utilized to
 196 obtain the dynamic stiffness matrix in the y -direction. The vertical trans-
 197 lational and rotational springs at $\eta = -1$ are denoted as $k_{\eta=-1}^v$ and $k_{\eta=-1}^r$,
 198 respectively, while those at $\eta = 1$ are represented by $k_{\eta=1}^v$ and $k_{\eta=1}^r$.

199 Following the same steps as for the x -direction, the Rayleigh principle is
 200 expressed in the form:

$$\delta U = \omega_y^2 \delta T_0, \quad (30)$$

201 from which the governing differential equation in the y -direction for ψ is
 202 obtained as:

$$\frac{d^4\psi}{d\eta^4} + \frac{2}{\chi^2} \left(\frac{D_{12}J_2}{D_{22}J_1} - 2 \frac{D_{66}J_3}{D_{22}J_1} \right) \frac{d^2\psi}{d\eta^2} + \left(\frac{D_{11}J_4}{\chi^4 D_{22}J_1} - \frac{b^4 D_{11}}{D_{22}} \Omega_y^4 \right) \psi = 0, \quad (31)$$

203 where $\Omega_y = \sqrt[4]{\omega_y^2 \rho h / D_{11}}$. By substituting $\psi(\eta) = Be^{\lambda\eta}$ into Equation (31),
 204 yields:

$$\lambda^4 + \frac{2}{\chi^2} \left(\frac{D_{12}J_2}{D_{22}J_1} - 2 \frac{D_{66}J_3}{D_{22}J_1} \right) \lambda^2 + \left(\frac{D_{11}J_4}{\chi^4 D_{22}J_1} - \frac{b^4 D_{11}}{D_{22}} \Omega_y^4 \right) = 0. \quad (32)$$

205 The solution for λ can be expressed as:

$$\lambda_{1,2} = \pm i\alpha_2, \quad \lambda_{3,4} = \pm \beta_2, \quad (33)$$

²⁰⁶ where,

$$\alpha_2 = \frac{1}{\chi} \sqrt{\sqrt{\left(\frac{D_{12}J_2}{D_{22}J_1} - 2\frac{D_{66}J_3}{D_{22}J_1}\right)^2 - \frac{D_{11}J_4}{D_{22}J_1} + \frac{a^4 D_{11}}{D_{22}} \Omega_y^4} + \frac{D_{12}J_2}{D_{22}J_1} - 2\frac{D_{66}J_3}{D_{22}J_1}}, \quad (34a)$$

$$\beta_2 = \frac{1}{\chi} \sqrt{\sqrt{\left(\frac{D_{12}J_2}{D_{22}J_1} - 2\frac{D_{66}J_3}{D_{22}J_1}\right)^2 - \frac{D_{11}J_4}{D_{22}J_1} + \frac{a^4 D_{11}}{D_{22}} \Omega_y^4} - \frac{D_{12}J_2}{D_{22}J_1} + 2\frac{D_{66}J_3}{D_{22}J_1}}. \quad (34b)$$

²⁰⁷ Similarly, from the shear force and bending moment equilibrium, and by
²⁰⁸ denoting $k_\eta^{v*} \equiv \frac{2b^3 k_\eta^v}{D_{22}}$, $k_\eta^{r*} \equiv \frac{2b k_\eta^r}{D_{22}}$, $S_{\alpha_2} \equiv \sin \alpha_2$, $C_{\alpha_2} \equiv \cos \alpha_2$, $Sh_{\beta_2} \equiv \sinh \beta_2$,
²⁰⁹ and $Ch_{\beta_2} \equiv \cosh \beta_2$, we obtain:

$$\begin{bmatrix} \zeta_1 C_{\alpha_2} - k_{\eta=-1}^{v*} S_{\alpha_2} & \zeta_1 S_{\alpha_2} + k_{\eta=-1}^{v*} C_{\alpha_2} & \zeta_2 Ch_{\beta_2} - k_{\eta=-1}^{v*} Sh_{\beta_2} \\ \zeta_3 S_{\alpha_2} + k_{\eta=-1}^{r*} \alpha_2 C_{\alpha_2} & -\zeta_3 C_{\alpha_2} + k_{\eta=-1}^{r*} \alpha_2 S_{\alpha_2} & \zeta_4 Sh_{\beta_2} + k_{\eta=-1}^{r*} \beta_2 Ch_{\beta_2} \\ -\zeta_1 C_{\alpha_2} + k_{\eta=1}^{v*} S_{\alpha_2} & \zeta_1 S_{\alpha_2} + k_{\eta=1}^{v*} C_{\alpha_2} & -\zeta_2 Ch_{\beta_2} + k_{\eta=1}^{v*} Sh_{\beta_2} \\ \zeta_3 S_{\alpha_2} + k_{\eta=1}^{r*} \alpha_2 C_{\alpha_2} & \zeta_3 C_{\alpha_2} - k_{\eta=1}^{r*} \alpha_2 S_{\alpha_2} & \zeta_4 Sh_{\beta_2} + k_{\eta=1}^{r*} \beta_2 Ch_{\beta_2} \\ -\zeta_2 Sh_{\beta_2} + k_{\eta=-1}^{v*} Ch_{\beta_2} & & \\ -\zeta_4 Ch_{\beta_2} - k_{\eta=-1}^{r*} \beta_2 Sh_{\beta_2} & & \\ -\zeta_2 Sh_{\beta_2} + k_{\eta=1}^{v*} Ch_{\beta_2} & & \\ \zeta_4 Ch_{\beta_2} + k_{\eta=1}^{r*} \beta_2 Sh_{\beta_2} & & \end{bmatrix} \begin{Bmatrix} B_1 \\ B_2 \\ B_3 \\ B_4 \end{Bmatrix} = \begin{Bmatrix} 0 \\ 0 \\ 0 \\ 0 \end{Bmatrix}, \quad (35)$$

²¹⁰ or,

$$\mathbf{R}_y \mathbf{B} = \mathbf{0}, \quad (36)$$

²¹¹ where,

$$\begin{aligned}\zeta_1 &= -\alpha_2^3 - \left(\frac{4D_{66}J_3}{\chi^2 D_{22}J_1} - \frac{D_{12}J_2}{\chi^2 D_{22}J_1} \right) \alpha_2, \\ \zeta_2 &= \beta_2^3 - \left(\frac{4D_{66}T_3}{\chi^2 D_{22}J_1} - \frac{D_{12}J_2}{\chi^2 D_{22}J_1} \right) \beta_2, \\ \zeta_3 &= -\alpha_2^2 + \frac{D_{12}J_2}{\chi^2 D_{22}J_1}, \\ \zeta_4 &= \beta_2^2 + \frac{D_{12}J_2}{\chi^2 D_{22}J_1}.\end{aligned}\tag{37}$$

²¹² With the help of Equation (9b), the vertical displacement and rotation cor-
²¹³ responding to the mode shape ψ along the y -direction at the edges $\eta = -1$
²¹⁴ and $\eta = 1$ can be expressed as:

$$\begin{Bmatrix} \psi_{\eta=-1} \\ \frac{d\psi}{d\eta}_{\eta=-1} \\ \psi_{\eta=1} \\ \frac{d\psi}{d\eta}_{\eta=1} \end{Bmatrix} = \begin{bmatrix} -S_{\alpha_2} & C_{\alpha_2} & -Sh_{\beta_2} & Ch_{\beta_2} \\ \alpha_2 C_{\alpha_2}/b & \alpha_2 S_{\alpha_2}/b & \beta_2 Ch_{\beta_2}/b & -\beta_2 Sh_{\beta_2}/b \\ S_{\alpha_2} & C_{\alpha_2} & Sh_{\beta_2} & Ch_{\beta_2} \\ \alpha_2 C_{\alpha_2}/b & -\frac{\alpha_2 S_{\alpha_2}}{b} & \beta_2 Ch_{\beta_2}/b & \beta_2 Sh_{\beta_2}/b \end{bmatrix} \begin{Bmatrix} B_1 \\ B_2 \\ B_3 \\ B_4 \end{Bmatrix}, \tag{38}$$

²¹⁵ or,

$$\delta_y = \mathbf{Q}_y \mathbf{B}. \tag{39}$$

²¹⁶ Solving for the eigenvector \mathbf{B} , and then substituting into Equation (36), we
²¹⁷ obtain:

$$\mathbf{R}_y \mathbf{B} = \mathbf{R}_y \mathbf{Q}_x^{-1} \delta_y = \mathbf{0}, \tag{40}$$

²¹⁸ where the dynamic stiffness matrix, denoted as $\mathbf{K}_y = \mathbf{R}_y \mathbf{Q}_y^{-1}$, can be ob-
²¹⁹ tained from Equation (40).

²²⁰ Remarks

²²¹ (i) For the SOV methods, six independent unknown eigenvalues ($\alpha_1, \beta_1,$
²²² $\Omega_x, \alpha_2, \beta_2, \Omega_y$) need to be determined for each mode shape $\phi(\xi)\psi(\eta)$.

To solve these six variables, four eigenvalue equations are provided in Equations (20a), (20b), (34a) and (34b), while the remaining two transcendental eigenvalue equations are obtained from the determinants of \mathbf{R}_x in Equation (25) for the x -direction and \mathbf{R}_y in Equation (36) for the y -direction, respectively. For classical boundary conditions such as simply supported (S), clamped (C), guided (G), and free (F) edges, these two transcendental equations have been simplified and summarized in previous works [53–55]. However, the process of selecting appropriate transcendental equations for the existing 55 different boundary-condition combinations remains tedious, and further simplification becomes challenging when non-classical boundary conditions are applied. By simply setting the translational springs (k^v) and rotational springs (k^r) along the x - or y -direction edges to either zero or infinity, the classical boundary conditions can be recovered. In this case, the transcendental equations obtained from the determinants of \mathbf{R}_x and \mathbf{R}_y are identical to those summarized in the existing SOV methods.

(ii) In the existing SOV methods, numerical techniques such as the Newton–Raphson method, homotopy method and optimization methods method have been applied to solve these six unknown variables. Although all six eigenvalue equations can be solved simultaneously, the computation is very expensive and convergence issues may arise [56, 57]. Therefore, an iterative procedure [52, 56–59] is preferred, in which three eigenvalue equations corresponding to $(\alpha_1, \beta_1, \Omega_x)$ and the remaining three corresponding to $(\alpha_2, \beta_2, \Omega_y)$ are solved separately. In fact, by substituting Equations (20a) and (20b) into the eigenvalue equation corresponding to \mathbf{R}_x and Equations (34a) and (34b) into the eigenvalue equation corresponding to \mathbf{R}_y , two highly nonlinear eigenvalue equations, involving only one variable Ω_x and Ω_y , respectively, can be obtained. However, these equations are difficult to solve using conventional numerical methods. To address this issue, the dynamic

253 stiffness matrices $\mathbf{K}_x(\Omega_x)$ and $\mathbf{K}_y(\Omega_y)$ are developed, whose determi-
 254 nants are identical to the eigenvalue equations corresponding to $\mathbf{R}_x(\Omega_x)$
 255 and $\mathbf{R}_y(\Omega_y)$, respectively. In this case, the dynamic stiffness matrices
 256 $\mathbf{K}_x(\Omega_x)$ and $\mathbf{K}_y(\Omega_y)$ can be solved efficiently using the W–W algo-
 257 rithm, which enhances computational robustness and ensures that no
 258 frequencies are missed.

259 **3. Frequency and mode shape computation**

260 The dynamic stiffness matrices $\mathbf{K}_x(\Omega_x)$ and $\mathbf{K}_y(\Omega_y)$ serve as the eigen-
 261 value equations for Ω_x and Ω_y , respectively, and a powerful W–W algorithm
 262 based on the SOV-DSM method is introduced in Section 3.1 to compute
 263 these eigenvalues. Section 3.2 proposes a novel technique to calculate the
 264 mode shapes. Finally, the iterative procedure for applying the proposed
 265 method is presented in Section 3.3.

266 *3.1. Wittrick–Williams algorithm and enhancement*

267 The Wittrick–Williams (W–W) algorithm [91] is an effective method for
 268 determining the natural frequencies from the dynamic stiffness matrix with
 269 high reliability. Instead of directly solving the equations, the algorithm com-
 270 putes the total number J of natural frequencies below a given frequency ω^* ,
 271 which is represented as:

$$J(\omega^*) = J_0(\omega^*) + s\{\mathbf{K}^\Delta(\omega^*)\} = J_0(\omega^*) + J_k(\omega^*), \quad (41)$$

272 where J_0 represents the number of natural frequencies of the structure with
 273 all ends fully clamped, \mathbf{K}^Δ is the upper triangular matrix obtained from the
 274 dynamic stiffness matrix \mathbf{K} after applying Gaussian elimination, and $J_k(\omega^*)$
 275 denotes the number of negative elements in the leading diagonal of \mathbf{K}^Δ .

276 It should be noted that the J_0 count is a crucial aspect when applying the
 277 W–W algorithm. Many previous studies use a sufficiently fine mesh or enough
 278 terms in series expansions to capture all fully clamped natural frequencies,

279 ensuring computational accuracy [67]. However, this approach can make the
 280 application process cumbersome. To address this issue, the fully clamped
 281 problem can be replaced with a simply supported problem, where the Navier
 282 solution for the simply supported plate is used to count J_0 [71]. Nevertheless,
 283 since analytical solutions in DSM methods involve an infinite series of Fourier
 284 terms, a sufficient number of truncation terms is required to ensure accuracy
 285 and convergence.

286 In fact, J_0 can be indirectly determined by evaluating the number of
 287 natural frequencies J of the structure under specific boundary conditions,
 288 which are generally different from the original boundary conditions [92]:

$$J_0(p_1, \omega^*) = J(\bar{p}_1, \omega^*) - J_k(\bar{p}_1, \omega^*), \quad (42)$$

289 where p_1 denotes the fully clamped supports, and \bar{p}_1 denotes specific sup-
 290 ports, which are typically simply supported, guided, or a combination of the
 291 two. For these specific boundary conditions, the eigenvalue equations of SOV
 292 type solution take the form of a single harmonic function. By substituting
 293 Equation (42) into Equation (41) we get the algorithm as:

$$J(p, \omega^*) = J(\bar{p}_1, \omega^*) - J_k(\bar{p}_1, \omega^*) + J_k(p, \omega^*) \quad (43)$$

294 where p represents the original boundary conditions of the structure. There-
 295 fore, the challenge of determining $J_0(p_1, \omega^*)$ can be transformed into the
 296 problem of solving $J(\bar{p}_1, \omega^*)$ instead.

297 By taking fully S-S boundary conditions as the basis, the eigenvalue equa-
 298 tion corresponding to the natural frequency parameter Ω_x can be obtained
 299 from the determinant of the coefficient matrix \mathbf{R}_x in Equation (24), as given
 300 by:

$$\sin 2\alpha_1 = 0. \quad (44)$$

301 With the help of Equations (20a) and (44), the closed-form solution of the
 302 n_x -th S-S boundary conditions frequency Ω_{x,n_x} for the given n_y -order $\psi_{n_y}(\eta)$

303 can be expressed as:

$$b\Omega_{x,n_x}^4 = \left[\left(\frac{n_x \pi}{2\chi} \right)^2 - \frac{D_{12}S_2}{D_{11}S_1} + 2 \frac{D_{66}S_3}{D_{11}S_1} \right]^2 - \left(\frac{D_{12}S_2}{D_{11}S_1} - 2 \frac{D_{66}S_3}{D_{11}S_1} \right)^2 + \frac{D_{22}S_4}{D_{11}S_1}. \quad (45)$$

304 For $\Omega_{x,n_x} \leq \Omega_x^* < \Omega_{x,n_{x+1}}$, $J(\bar{p}_1, \Omega_x^*) = n_x$.

305 Similarly, the closed-form solution of the n_y -th S-S boundary conditions
306 frequency Ω_{y,n_y} for the given n_x -order $\phi_{n_x}(\xi)$ can be expressed as:

$$a\Omega_{y,n_y}^4 = \frac{D_{22}}{D_{11}} \left\{ \left[\left(\frac{n_y \pi \chi}{2} \right)^2 - \frac{D_{12}T_2}{D_{22}T_1} + 2 \frac{D_{66}T_3}{D_{22}T_1} \right]^2 - \left(\frac{D_{12}T_2}{D_{22}T_1} - 2 \frac{D_{66}T_3}{D_{22}T_1} \right)^2 + \frac{D_{11}T_4}{D_{22}T_1} \right\}. \quad (46)$$

307 For $\Omega_{y,n_y} \leq \Omega_y^* < \Omega_{y,n_{y+1}}$, $J(\bar{p}_1, \Omega_y^*) = n_y$.

308 It should be noted that the G-G boundary conditions have the same eigen-
309 value equations with the S-S boundary conditions, thus the G-G boundary
310 conditions frequencies can also be directly obtained from Equations (45)
311 and (46). The closed-form expression for the S-G boundary conditions can
312 be found in Appendix B.

313 According to the relationships $\Omega_x^4 = \omega_x^2 \rho h / D_{11}$ and $\Omega_y^4 = \omega_y^2 \rho h / D_{11}$, the
314 values of $J(\bar{p}_1, \omega_x^*)$ and $J(\bar{p}_1, \omega_y^*)$ can be derived from $J(\bar{p}_1, \Omega_x^*)$ and $J(\bar{p}_1, \Omega_y^*)$,
315 respectively. Therefore, this enhanced W-W algorithm can be applied to
316 estimate the lower and upper bounds of the frequency range, denoted as ω_l
317 and ω_u , yielding an approximation for the frequency $\omega_a \in (\omega_l, \omega_u)$ to arbitrary
318 precision.

319 3.2. Mode shape computation

320 The mode shape coefficients A_1 to A_4 and B_1 to B_4 in the eigenvectors
321 **A** and **B** for all classic boundary conditions are provided in [53, 54]. Alter-

natively, these coefficients can also be obtained through a simple numerical method, which this work presents as an approach. Here, we illustrate solving the eigenvector \mathbf{A} as an example. By assuming the exact natural frequency as ω_k , we can expand the coefficient matrix \mathbf{R}_x in Equation (24) using a first-order Taylor series about ω_a :

$$\mathbf{R}_{x,k}(\omega_k)\mathbf{A}_k = \mathbf{R}_{x,a}\mathbf{A}_k + (\omega_k - \omega_a)\mathbf{R}'_{x,a}\mathbf{A}_k + O((\omega_k - \omega_a)^2) = 0. \quad (47)$$

Ignoring higher-order terms, an eigenvalue problem can be derived from Equation (47):

$$(\mathbf{R}'_{x,a})^{-1}\mathbf{R}_{x,a}\mathbf{A} = (\omega_a - \omega_k)\mathbf{A} = \tau\mathbf{A}. \quad (48)$$

This eigenvalue problem can be solved using the inverse iteration procedure [94]:

$$\bar{\mathbf{A}}^{(i+1)} = \mathbf{R}_{x,a}^{-1}\mathbf{R}'_{x,a}\mathbf{A}^{(i)}, \quad (49)$$

where the initial guess for $\mathbf{A}^{(0)}$ is a column vector consisting of four randomly generated elements, each of which falls within the range (0,1). The updated eigenvalue for the next step can be obtained as:

$$\tau^{(i+1)} = \frac{1}{\bar{A}_j^{(i+1)}}, \quad (50)$$

where,

$$|\bar{A}_j^{(i+1)}| = \max(|\bar{A}_1^{(i+1)}|, |\bar{A}_2^{(i+1)}|, |\bar{A}_3^{(i+1)}|, |\bar{A}_4^{(i+1)}|). \quad (51)$$

The updated eigenvector can be obtained as:

$$\mathbf{A}^{(i+1)} = \tau^{(i+1)}\bar{\mathbf{A}}^{(i+1)}. \quad (52)$$

³³⁶ The procedure can be controlled by the error tolerance ϵ or maximum allowed
³³⁷ steps i_{\max} :

$$\max | A_n^{(i+1)} - A_n^{(i)} | < \epsilon, \quad (53a)$$

$$i = i_{\max}. \quad (53b)$$

³³⁸ Note that the mode shape coefficients A_1 to A_4 obtained from $\mathbf{A}^{(i+1)}$ are
³³⁹ applied for the elastically restrained boundary conditions.

³⁴⁰ 3.3. Application procedure

³⁴¹ The procedure of the proposed method is as follows:

- ³⁴² • **Step 1** Assume initial integral parameters $I_1^{(0)}, I_2^{(0)}, I_3^{(0)}$, and $I_4^{(0)}$ in the
³⁴³ y -direction. Using the given boundary conditions at $\xi = -1$ and $\xi = 1$,
³⁴⁴ determine $\mathbf{K}_x^{(0)}$ from Equation (29). Then, apply the computational
³⁴⁵ algorithms in Section 3.1 to compute the lower and upper bounds of the
³⁴⁶ n_x -th non-dimensional frequency parameter, $2a\Omega_{l,x,n_x}^{(0)}$ and $2a\Omega_{u,x,n_x}^{(0)}$,
³⁴⁷ and take the average $2a\Omega_{x,n_x}^{(0)} = (2a\Omega_{l,x,n_x}^{(0)} + 2a\Omega_{u,x,n_x}^{(0)})/2$ along with its
³⁴⁸ corresponding mode shape $\phi_{n_x}^{(0)}$, where $n_x = 1, 2, 3, \dots$.
- ³⁴⁹ • **Step 2** Use $\phi_{n_x}^{(0)}$ as the prescribed mode to determine $\mathbf{K}_y^{(1)}$ in Equa-
³⁵⁰ tion (40), considering the boundary conditions at $\eta = -1$ and $\eta = 1$.
³⁵¹ Apply the computational algorithms to obtain the n_y -th frequency pa-
³⁵² rameter $2a\Omega_{y,n_y}^{(1)}$ and its corresponding mode shape $\psi_{n_y}^{(1)}$, where $n_y =$
³⁵³ $1, 2, 3, \dots$. This completes the first iteration cycle.
- ³⁵⁴ • **Step 3** Use $\psi_{n_y}^{(1)}$ as the prescribed n_y -th mode shape in the y -direction to
³⁵⁵ compute $\mathbf{K}_x^{(1)}$ from Equation (29), then determine the n_x -th frequency
³⁵⁶ parameter $2a\Omega_{x,n_x}^{(1)}$ and its corresponding mode shape $\phi_{n_x}^{(1)}$.
- ³⁵⁷ • **Step 4** Use $\phi_{n_x}^{(1)}$ as the prescribed mode in the x -direction to com-
³⁵⁸ pute the n_y -th frequency parameter $2a\Omega_{y,n_y}^{(2)}$ and its corresponding mode
³⁵⁹ shape $\psi_{n_y}^{(2)}$, completing the second iteration cycle.

- 360 • **Step 5** Stop the iteration if $|2a\Omega_{x,n_x}^{(i)} - 2a\Omega_{x,n_x}^{(i+1)}| \leq \Delta 2a\Omega$ or $|2a\Omega_{y,n_y}^{(i)} -$
 361 $2a\Omega_{y,n_y}^{(i+1)}| \leq \Delta 2a\Omega$, where $\Delta 2a\Omega = 2a\Omega_u - 2a\Omega_l$. Here, $2a\Omega_l$ and $2a\Omega_u$
 362 are the lower and upper bounds of the frequency parameter range,
 363 within which the actual frequency parameter $2a\Omega$ lies, i.e., $2a\Omega \in$
 364 $(2a\Omega_l, 2a\Omega_u)$. The quantity $\Delta 2a\Omega$ represents the frequency parameter interval used in the W-W algorithm.
 365
- 366 • **Step 6** Finally, construct the (n_x, n_y) -th mode shape as $w(\xi, \eta) =$
 367 $\phi_{n_x}(\xi)\psi_{n_y}(\eta)$ using Equation (8).

368 **Remarks**

- 369 (i) The traditional W-W algorithm requires a prior expression of $J_0(p_1)$
 370 under the C-C boundary conditions (p_1). However, the transcendental
 371 eigenvalue equation for C-C boundaries is complex, making it difficult
 372 to obtain a closed-form solution for the $J_0(p_1)$ term. To overcome
 373 this difficulty, $J_0(p_1)$ can be indirectly determined if the $J(\bar{p}_1)$ term is
 374 known, where the reference boundary condition \bar{p}_1 may correspond to
 375 any other, more tractable boundary condition. Consequently, to apply
 376 the W-W algorithm, at least one prior solution for a specific bound-
 377 ary condition is required. Thanks to the SOV solution, the S-S, G-G,
 378 and S-G boundary conditions yield the simplest eigenvalue equations,
 379 involving only a single sine or cosine function. Therefore, an explicit
 380 closed-form expression of $J(\bar{p}_1)$ can be readily obtained when \bar{p}_1 corre-
 381 sponds to one of these boundary conditions. In numerical calculations,
 382 to approximate infinite stiffness, the translational springs (k^v) and ro-
 383 tational springs (k^r) are assigned sufficiently large values.
- 384 (ii) In the existing SOV methods, the mode shape coefficients A_1 to A_4 and
 385 B_1 to B_4 are obtained from different types of transcendental eigenvalue
 386 equations for each boundary condition, resulting in distinct expressions

387 for different boundary conditions. However, the dynamic stiffness ma-
388 trix \mathbf{K} is applicable to all boundary conditions. Therefore, a general
389 approach is developed to compute the mode shape coefficients for arbi-
390 trary boundary conditions, and a novel yet simple numerical technique
391 has been introduced to implement this procedure efficiently.

392 **4. Numerical Results**

393 This section aims to validate the SOV-DSM method by comparing its
394 results with some existing methods. In Section 4.1, the results are compared
395 with those obtained from the extended SOV method under classical boundary
396 conditions. In Section 4.2, the results are further compared with the finite
397 integral transform method and numerical methods for rotationally restrained
398 boundary conditions.

399 For all numerical calculations, the initial integral parameters are assumed
400 as $I_1^{(0)} = 1$, $I_2^{(0)} = 1$, $I_3^{(0)} = 1$, and $I_4^{(0)} = 10$ in the y -direction, serving as
401 the starting point of **Step 1** for any mode in all boundary conditions. \bar{p}_1 is
402 selected as the S–S boundary condition. In this section, the interval between
403 the upper and lower bounds of the non-dimensional frequency parameter,
404 $2a\Delta\Omega$, is set to 0.005, although any desired level of precision can be used.
405 According to our numerical calculations, two iteration cycles are generally
406 sufficient to meet the convergence requirement (i.e., $|2a\Omega_x^{(i)} - 2a\Omega_x^{(i+1)}| \leq$
407 $\Delta 2a\Omega$ or $|2a\Omega_y^{(i)} - 2a\Omega_y^{(i+1)}| \leq \Delta 2a\Omega$) for most cases, with at most three
408 cycles required when applying the iterative procedure in Section 3.3.

409 *4.1. Classical boundary conditions*

410 In this subsection, the proposed method is validated by comparison with
411 the extended SOV method [53]. The properties of the orthotropic plate,
412 consistent with those in [53], are as follows: $E_1 = 185$ GPa, $E_2 = 10.5$ GPa,
413 $G_{12} = 7.3$ GPa, $\rho = 1600$ kg m⁻¹, and $\nu_{12} = 0.28$.

414 The translational springs (k^v) and rotational springs (k^r) along all edges
 415 can be set to zero or infinity (represented as 1×10^{15} N m⁻¹ in the numerical
 416 calculations of this study) to obtain different classic boundary conditions.

417 The results for SSSS, SCSF, GCGC, CCCC, SSCC, SCCC, GGCC, CCFF,
 418 CFCF, CFFF, and FFFF boundary conditions are presented in Tables 1
 419 to 3. These results demonstrate high accuracy compared to the extended
 420 SOV method, with difference remaining smaller than the frequency parame-
 421 ter interval $2a\Delta\Omega = 0.005$. The frequency parameters in both directions are
 422 equal ($2a\Omega_x - 2a\Omega_y = 0$) in almost all cases, with a few exceptions where
 423 $2a\Omega_x - 2a\Omega_y = 0.005$. In fact, higher accuracy compared to the extended
 424 SOV method can be achieved if the frequency parameter interval $2a\Delta\Omega$ is
 425 set smaller than 0.005. It should be noted that the accuracy improves only
 426 by reducing $2a\Delta\Omega$, and no additional iterations are required according to
 427 our calculations. Section 4.1 shows the first six nonzero mode shapes of a
 428 square orthotropic plate with FFFF boundary conditions, where the mode
 429 shape coefficients are calculated using the numerical method developed in
 430 this study. Instead of selecting fixed expressions for the mode shape coeffi-
 431 cients based on specific boundary conditions, our method is applicable to all
 432 boundary conditions.

433 *4.2. Rotational spring-supported edges*

434 In this subsection, rectangular orthotropic plates with rotational spring-
 435 supported edges with no translations ($k_\xi^v = k_\eta^v = \infty$) are examined. The
 436 dimensionless rotational stiffness coefficients are defined as:

$$r_\xi = \frac{2ak_\xi^r}{D_{11}}, \quad (54a)$$

$$r_\eta = \frac{2bk_\eta^r}{D_{22}}. \quad (54b)$$

437 The first example considers a square isotropic plate with all four edges ro-
 438 tationally restrained. The vertical translational springs along the four edges

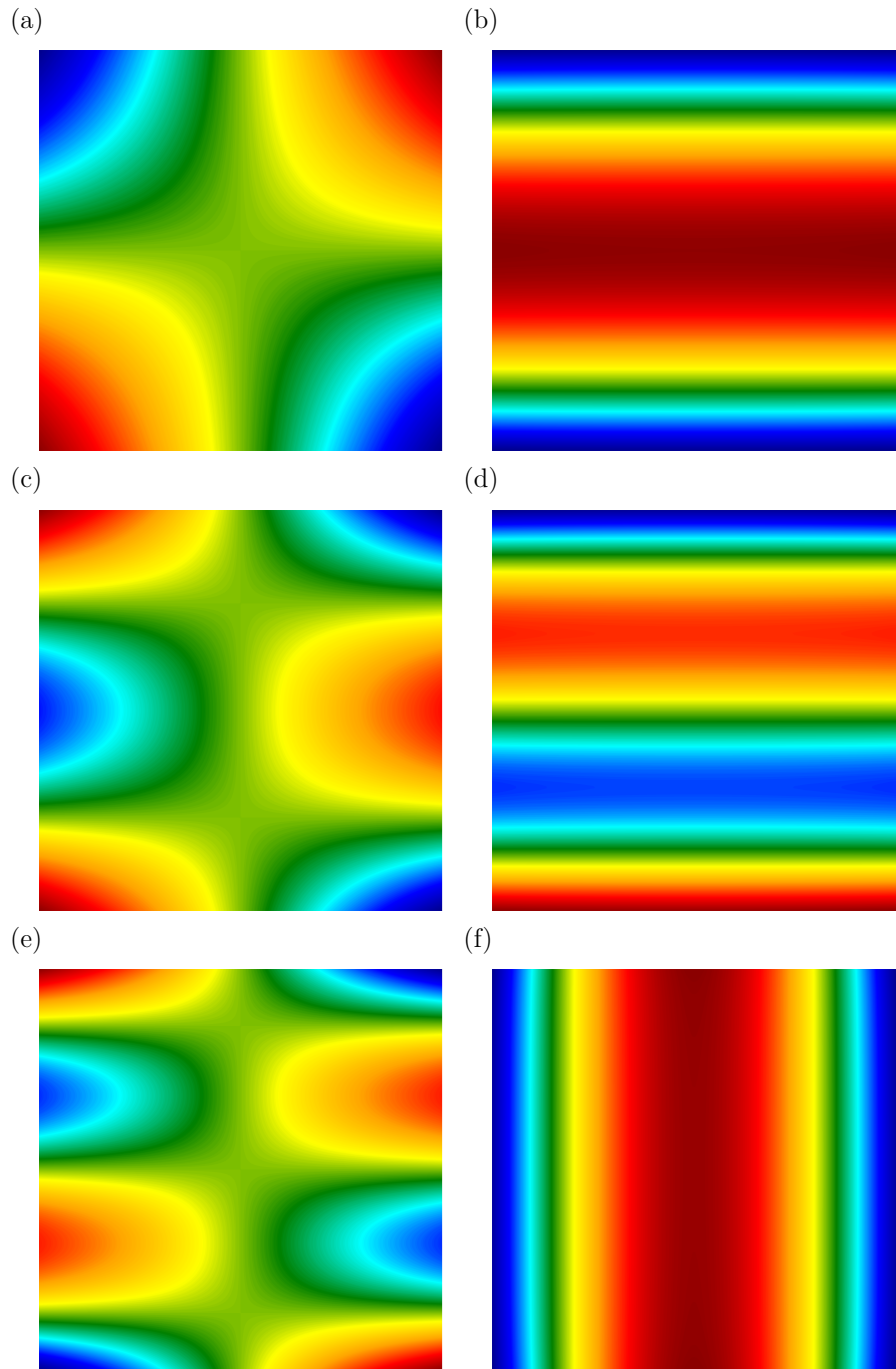


Figure 2: The first six nonzero mode shapes of a square orthotropic plate with FFFF boundary conditions: (a) the first mode; (b) the second mode; (c) the third mode; (d) the fourth mode; (e) the fifth mode; (f) the sixth mode.

Table 1: The first seven frequency parameter $2a\Omega$ of orthotropic rectangular plates with SSSS, SCSF and GCGC boundary conditions.

BCs	χ	Mode	$2a\Omega_x = 2a\Omega_y = 2a\sqrt[4]{\rho h \omega^2 / D_{11}}$						
			1	2	3	4	5	6	7
SSSS	0.5	Mode number	(1,1)	(1,2)	(1,3)	(1,4)	(1,5)	(1,6)	(1,7)
		extended SOV 53	3.1807	3.3190	3.5938	4.0135	4.5495	5.1635	5.8265
		Present	3.1825	3.3225	3.5975	4.0175	4.5525	5.1625	5.8275
	1	Mode number	(1,1)	(1,2)	(1,3)	(2,1)	(1,4)	(2,2)	(2,3)
		extended SOV 53	3.3190	4.0135	5.1635	6.3615	6.5200	6.6379	7.1876
		Present	3.3175	4.0175	5.1625	6.3625	6.5175	6.6375	7.1875
	1.5	Mode number	(1,1)	(1,2)	(2,1)	(2,2)	(1,3)	(2,3)	(1,4)
		extended SOV 53	3.5938	5.1635	6.4698	7.1876	7.2331	8.5389	9.4352
		Present	3.5975	5.1675	6.4725	7.1875	7.2325	8.5375	9.4375
SCSF	0.5	Mode number	(1,1)	(1,2)	(1,3)	(1,4)	(1,5)	(1,6)	(1,7)
		extended SOV 53	3.1516	3.2451	3.4588	3.8131	4.2950	4.8711	5.5087
		Present	3.1525	3.2475	3.4575	3.8175	4.2925	4.8725	5.5075
	1	Mode number	(1,1)	(1,2)	(1,3)	(1,4)	(2,1)	(2,2)	(2,3)
		extended SOV 53	3.1908	3.6428	4.5972	5.8599	6.3033	6.4901	6.9177
		Present	3.1925	3.6425	4.5975	5.8575	6.3025	6.4925	6.9175
	1.5	Mode number	(1,1)	(1,2)	(1,3)	(2,1)	(2,2)	(2,3)	(1,4)
		extended SOV 53	3.2710	4.3430	6.2157	6.3337	6.8043	7.8718	8.3518
		Present	3.2725	4.3425	6.2175	6.3325	6.8025	7.8725	8.3525
GCGC	0.5	Mode number	(1,1)	(1,2)	(1,3)	(2,1)	(2,2)	(1,4)	(2,3)
		extended SOV 53	1.1544	1.9166	2.6835	3.1983	3.3890	3.4501	3.7372
		Present	1.1525	1.9175	2.6825	3.1975	3.3875	3.4525	3.7375
	1	Mode number	(1,1)	(2,1)	(1,2)	(2,2)	(1,3)	(2,3)	(3,1)
		extended SOV 53	2.3087	3.4900	3.8331	4.4682	5.3669	5.7736	6.3967
		Present	2.3075	3.4875	3.8325	4.4675	5.3675	5.7725	6.3975
	1.5	Mode number	(1,1)	(2,1)	(1,2)	(2,2)	(3,1)	(3,2)	(1,3)
		extended SOV 53	3.4631	4.1353	5.7497	6.0981	6.6049	7.6449	8.0504
		Present	3.4625	4.1325	5.7475	6.0975	6.6075	7.6425	8.0525

Table 2: The first seven frequency parameter $2a\Omega$ of orthotropic rectangular plates with CCCC, SSCC, SCCC and GGCC boundary conditions.

BCs	χ	Mode	$2a\Omega_x = 2a\Omega_y = 2a\sqrt[4]{\rho h \omega^2 / D_{11}}$						
			1	2	3	4	5	6	7
CCCC	0.5	Mode number	(1,1)	(1,2)	(1,3)	(1,4)	(1,5)	(1,6)	(1,7)
		extended SOV 53	4.7500	4.8208	4.9682	5.2177	5.5791	6.0430	6.5892
		Present	4.7475	4.8225	4.9725	5.2175	5.5825	6.0425	6.5875
	1	Mode number	(1,1)	(1,2)	(1,3)	(1,4)	(2,1)	(2,2)	(2,3)
		extended SOV 53	4.8579	5.3546	6.2819	7.4972	7.9193	8.1490	8.6054
		Present	4.8575	5.3575	6.2875	7.4975	7.9175	8.1475	8.6075
	1.5	Mode number	(1,1)	(1,2)	(2,1)	(1,3)	(2,2)	(2,3)	(1,4)
		extended SOV 53	5.1581	6.5412	8.0409	8.4945	8.7204	9.9793	10.6460
		Present	5.1575	6.5375	8.0425	8.4975	8.7175	9.9775	10.6425
SSCC	0.5	Mode number	(1,1)	(1,2)	(1,3)	(1,4)	(1,5)	(1,6)	(1,7)
		extended SOV 53	3.9542	4.0520	4.2525	4.5785	5.0254	5.5682	6.1789
		Present	3.9575	4.0525	4.2475	4.5775	5.0225	5.5725	6.1825
	1	Mode number	(1,1)	(1,2)	(1,3)	(1,4)	(2,1)	(2,2)	(2,3)
		extended SOV 53	4.0745	4.6606	5.7009	6.9940	7.1396	7.3894	7.8881
		Present	4.0775	4.6625	5.7025	6.9925	7.1375	7.3875	7.8875
	1.5	Mode number	(1,1)	(1,2)	(2,1)	(1,3)	(2,2)	(2,3)	(1,4)
		extended SOV 53	4.3602	5.8384	7.2531	7.8560	7.9481	9.2515	10.0366
		Present	4.3625	5.8325	7.2525	7.8575	7.9525	9.2525	10.0325
SCCC	0.5	Mode number	(1,1)	(1,2)	(1,3)	(1,4)	(1,5)	(1,6)	(1,7)
		extended SOV 53	3.9596	4.0745	4.3027	4.6606	5.1361	5.7009	6.3271
		Present	3.9575	4.0725	4.3025	4.6625	5.1325	5.7025	6.3325
	1	Mode number	(1,1)	(1,2)	(1,3)	(2,1)	(1,4)	(2,2)	(2,3)
		extended SOV 53	4.1349	4.8478	5.9805	7.1541	7.3192	7.4478	8.0121
		Present	4.1325	4.8475	5.9825	7.1525	7.3175	7.4475	8.0125
	1.5	Mode number	(1,1)	(1,2)	(2,1)	(2,2)	(1,3)	(2,3)	(3,1)
		extended SOV 53	4.5824	6.2766	7.3116	8.1528	8.3705	9.5986	10.3507
		Present	4.5825	6.2775	7.3125	8.1525	8.3725	9.5975	10.3525
GGCC	0.5	Mode number	(1,1)	(1,2)	(1,3)	(1,4)	(1,5)	(1,6)	(1,7)
		extended SOV 53	2.3750	2.4841	2.7895	3.2946	3.9226	4.6123	5.3326
		Present	2.3725	2.4875	2.7925	3.2975	3.9225	4.6075	5.3325
	1	Mode number	(1,1)	(1,2)	(1,3)	(2,1)	(2,2)	(1,4)	(2,3)
		extended SOV 53	2.4290	3.1410	4.4293	5.5202	5.7315	5.8801	6.2606
		Present	2.4325	3.1425	4.4325	5.5225	5.7325	5.8775	6.2625
	1.5	Mode number	(1,1)	(1,2)	(2,1)	(2,2)	(1,3)	(2,3)	(3,1)
		extended SOV 53	2.5790	4.2472	5.5565	6.1533	6.4347	7.5231	8.6732
		Present	2.5825	4.2475	5.5575	6.1525	6.4325	7.5225	8.6725

Table 3: The first seven nonzero frequency parameter $2a\Omega$ of orthotropic rectangular plates with CCFF, CFCF, CFFF and FFFF boundary conditions.

BCs	χ	Mode	$2a\Omega_x = 2a\Omega_y = 2a\sqrt[4]{\rho h \omega^2 / D_{11}}$						
			1	2	3	4	5	6	7
CCFF	0.5	Mode number	(1,1)	(1,2)	(1,3)	(1,4)	(1,5)	(1,6)	(2,1)
		extended SOV 53	1.8978	2.0905	2.4925	3.0563	3.7110	4.4117	4.7029
		Present	1.8975	2.0925	2.4925	3.0575	3.7125	4.4125	4.7025
	1	Mode number	(1,1)	(1,2)	(1,3)	(2,1)	(2,2)	(1,4)	(2,3)
		extended SOV 53	1.9930	2.7895	4.0733	4.7338	5.0652	5.5128	5.7419
		Present	1.9925	2.7875	4.0725	4.7325	5.0675	5.5125	5.7425
	1.5	Mode number	(1,1)	(1,2)	(2,1)	(2,2)	(1,3)	(2,3)	(3,1)
		extended SOV 53	2.1780	3.7411	4.7931	5.5758	5.8895	7.0263	7.9006
		Present	2.1775	3.7425	4.7925	5.5725	5.8875	7.0275	7.9025
CFCF	0.5	Mode number	(1,1)	(1,2)	(1,3)	(1,4)	(1,5)	(1,6)	(1,7)
		extended SOV 53	4.7297	4.7427	4.7881	4.8819	5.0478	5.3072	5.6694
		Present	4.7275	4.7425	4.7875	4.8825	5.0475	5.3075	5.6675
	1	Mode number	(1,1)	(1,2)	(1,3)	(1,4)	(1,5)	(1,6)	(2,1)
		extended SOV 53	4.7295	4.7817	5.0012	5.5348	6.4407	7.6182	7.8523
		Present	4.7275	4.7825	5.0025	5.5325	6.4425	7.6175	7.8525
	1.5	Mode number	(1,1)	(1,2)	(1,3)	(1,4)	(2,1)	(2,2)	(2,3)
		extended SOV 53	4.7292	4.8458	5.4221	6.7635	7.8518	7.9470	8.3021
		Present	4.7275	4.8475	5.4225	6.7625	7.8525	7.9475	8.3025
CFFF	0.5	Mode number	(1,1)	(1,2)	(1,3)	(1,4)	(1,5)	(1,6)	(1,7)
		extended SOV 53	1.8751	1.9439	2.1679	2.5657	3.1106	3.7486	4.4382
		Present	1.8775	1.9425	2.1675	2.5675	3.1125	3.7475	4.4375
	1	Mode number	(1,1)	(1,2)	(1,3)	(1,4)	(2,1)	(2,2)	(2,3)
		extended SOV 53	1.8750	2.1242	2.9077	4.1319	4.6937	4.8226	5.2263
		Present	1.8775	2.1225	2.9075	4.1325	4.6925	4.8225	5.2275
	1.5	Mode number	(1,1)	(1,2)	(1,3)	(2,1)	(2,2)	(2,3)	(1,4)
		extended SOV 53	1.8750	2.3402	3.8522	4.6935	4.9753	5.8314	5.9292
		Present	1.8775	2.3425	3.8525	4.6925	4.9775	5.8325	5.9275
FFFF	0.5	Mode number	(1,3)	(2,2)	(1,4)	(2,3)	(1,5)	(2,4)	(2,5)
		extended SOV 53	1.1540	1.4858	1.9157	2.1704	2.6821	2.7881	3.4093
		Present	1.1525	1.4875	1.9175	2.1725	2.6825	2.7875	3.4075
	1	Mode number	(2,2)	(1,3)	(2,3)	(1,4)	(2,4)	(3,1)	(3,2)
		extended SOV 53	2.1311	2.3082	3.2734	3.8320	4.4962	4.7298	4.9138
		Present	2.1325	2.3075	3.2725	3.8325	4.4975	4.7275	4.9125
	1.5	Mode number	(2,2)	(1,3)	(2,3)	(3,1)	(3,2)	(1,4)	(3,3)
		extended SOV 53	2.6277 ³⁰	3.4625	4.2915	4.7296	5.1259	5.7485	6.1588
		Present	2.6275	3.4625	4.2925	4.7275	5.1275	5.7475	6.1575

439 are numerically set as $k_{\xi=-1}^v = k_{\xi=1}^v = k_{\eta=-1}^v = k_{\eta=1}^v = 1 \times 10^{12}$ N m⁻¹. The
440 material properties are given as $D_{11} = D_{22} = D_3$ and $\nu_{12} = \nu_{21} = 0.3$.

441 Section 4.2 presents the frequency parameter $2a\Omega$ for different rotational
442 stiffness coefficients $r_\xi = r_\eta$ with values 0.1, 1, 10, 100, and 1000. Notably,
443 when $r_\xi = r_\eta = 0$ and $r_\xi = r_\eta = \infty$, the boundary conditions correspond to
444 SSSS and CCCC, respectively.

445 Interestingly, the results indicate that the frequencies Ω_x and Ω_y are not
446 strictly equal for some mode shapes under these boundary conditions. The
447 actual frequency Ω lies between Ω_x and Ω_y , which may be attributed to the
448 fact that Ω_x and Ω_y satisfy Rayleigh's principle in Equation (3), represent-
449 ing the weak-form governing equations, but do not necessarily satisfy the
450 strong-form governing equations in Equation (1). For a physical problem
451 with exact solutions, both Equations (1) and (3) must be satisfied. If this
452 condition is not met, applying Equation (3) still provides a viable approach
453 for approximating the exact solution of the plate. Thus, the exact frequency
454 can be estimated as $\Omega = (\Omega_x + \Omega_y)/2$. As shown in Section 4.2, the maxi-
455 mum difference between Ω and the analytical solutions of the finite integral
456 transform method reported in 95 is less than 1.3%. Figure 3 illustrates the
457 variation in mode shapes corresponding to the fundamental natural frequency
458 as the rotational stiffness $r_\xi = r_\eta$ increases from zero to ∞ , transitioning the
459 boundary conditions from SSSS to CCCC.

460 The next example considers a rectangular orthotropic plate with three
461 simply supported edges ($k_{\xi=-1}^r = k_{\xi=1}^r = k_{\eta=1}^r = 0$), while the edge at $\eta = -1$
462 is rotationally restrained. The material properties are consistent with those
463 in 95, where $2D_{11} = 2D_{22} = D_3$ and $\nu_{12} = \nu_{21} = 0.3$. Table 4 shows the
464 fundamental frequency results for different length ratios (b/a), comparing
465 them with those reported in 95. The maximum observed difference is 0.8%
466 when $r_{\eta=-1} = 10$.

467 Interestingly, in certain numerical calculations involving rotationally re-
468 strained boundary conditions, the variables α_1 and α_2 may take complex

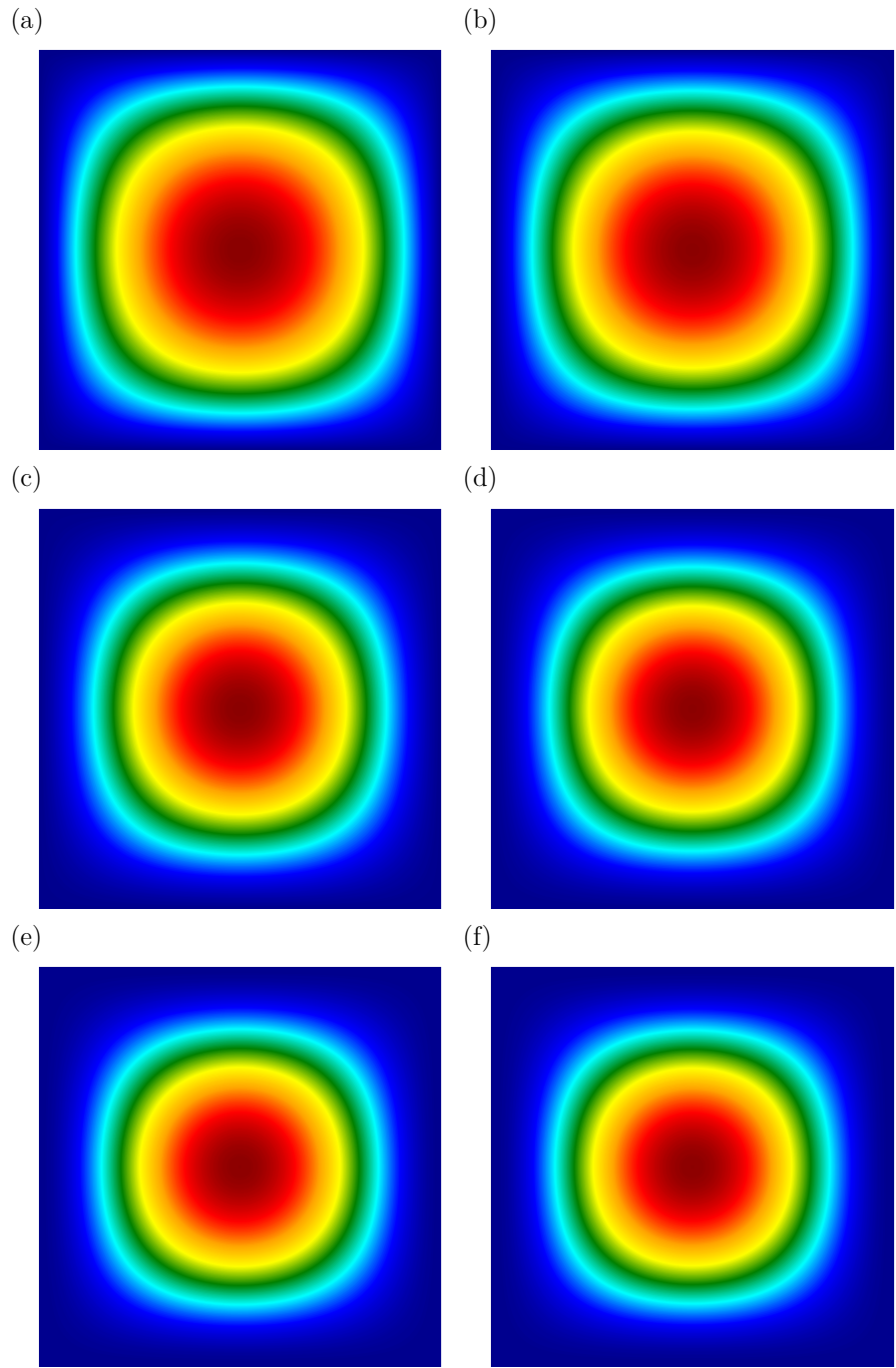


Figure 3: The first vibration mode shapes of a square isotropic plate with all four edges rotationally restrained, shown for different dimensionless rotational stiffness values $r_\xi = r_\eta$. (a) $r_\xi = r_\eta = 0$ (simply supported); (b) $r_\xi = r_\eta = 1$ (light rotational restraint); (c) $r_\xi = r_\eta = 10$ (moderate restraint); (d) $r_\xi = r_\eta = 20$; (e) $r_\xi = r_\eta = 100$ (firmly clamped); (f) $r_\xi = r_\eta = \infty$ (perfectly clamped edges).

r	Mode	$2a\Omega$					
		1	2	3	4	5	6
0.1	Mode number	(1,1)	(1,2)	(2,1)	(2,2)	(1,3)	(3,1)
	Ref.96	4.454	6.992	7.045	8.890	9.782	9.960
	Ref.95	4.465	7.039	7.039	8.897	9.945	9.945
	Present (Ω_x)	4.463	7.028	7.043	8.893	9.938	9.953
	Present (Ω_y)	4.463	7.043	7.028	8.893	9.953	9.938
	Present (Ω)	4.463	7.035	7.035	8.893	9.945	9.945
	Difference (%)	0.044	0.056	0.056	0.044	0.000	0.000
1	Mode number	(1,1)	(1,2)	(2,1)	(2,2)	(3,1)	(1,3)
	Ref.96	4.529	7.008	7.136	8.936	9.787	10.036
	Ref.95	4.637	7.155	7.155	8.991	10.029	10.030
	Present (Ω_x)	4.648	7.098	7.223	8.993	10.093	9.968
	Present (Ω_y)	4.648	7.223	7.098	8.993	9.968	10.098
	Present (Ω)	4.648	7.160	7.160	8.993	10.030	10.033
	Difference (%)	0.237	0.069	0.069	0.022	0.009	0.029
10	Mode number	(1,1)	(1,2)	(2,1)	(2,2)	(1,3)	(3,1)
	Ref.95	5.346	7.768	7.768	9.537	10.552	10.563
	Present (Ω_x)	5.413	7.718	7.953	9.598	10.448	10.782
	Present (Ω_y)	5.413	7.953	7.718	9.598	10.782	10.453
	Present (Ω)	5.413	7.835	7.835	9.598	10.615	10.618
	Difference (%)	1.253	0.862	0.862	0.639	0.597	0.520
	Mode number	(1,1)	(1,2)	(2,1)	(2,2)	(1,3)	(3,1)
100	Ref.96	5.895	8.326	8.422	10.167	10.957	11.297
	Ref.95	5.901	8.442	8.442	10.253	11.307	11.333
	Present (Ω_x)	5.913	8.428	8.473	10.258	11.293	11.373
	Present (Ω_y)	5.913	8.473	8.478	10.258	11.373	11.293
	Present (Ω)	5.913	8.450	8.450	10.258	11.333	11.333
	Difference (%)	0.203	0.094	0.094	0.048	0.229	0.000
	Mode number	(1,1)	(1,2)	(2,1)	(2,2)	(1,3)	(3,1)
1000	Ref.95	6.011	8.585	8.585	10.424	11.495	11.522
	Present (Ω_x)	5.988	8.553	8.553	10.388	11.463	11.478
	Present (Ω_y)	5.988	8.553	8.553	10.388	11.478	11.463
	Present (Ω)	5.988	8.553	8.553	10.388	11.470	11.470
	Difference (%)	0.382	0.372	0.372	0.345	0.217	0.451

469 values rather than being purely real. Consequently, the mode shape coeffi-
 470 cients A_1 , A_2 , B_1 , and B_2 become complex-valued, leading to \mathbf{R} and \mathbf{Q}^{-1}
 471 being complex matrices. However, the mode shapes $\phi(\xi)$ and $\psi(\eta)$ remain
 472 real-valued, and the dynamic stiffness matrix $\mathbf{K} = \mathbf{R}\mathbf{Q}^{-1}$ is a real symmet-
 473 ric matrix. Thus, the frequency Ω can be obtained by solving \mathbf{K} using this
 474 enhanced W-W algorithm provided in this study, which avoids solving the
 475 eigenvalue equations in both the real and complex domains.

Table 4: Fundamental frequency parameter $2a\Omega = 2a\sqrt[4]{\rho h\omega^2/D_{11}}$ of rectangular orthotropic plates with three edges simply supported ($k_{\xi=-1}^r = k_{\xi=1}^r = k_{\eta=1}^r = 0$) and the edge at $\eta = -1$ rotationally restrained.

		2aΩ				
b/a	$r_{\eta=-1}$	Ref.95	Present (Ω)	Present (Ω_x)	Present (Ω_y)	Difference (%)
0.5	0	7.530	7.523	7.523	7.523	0.092
	1	7.690	7.700	7.588	7.813	0.130
	10	8.250	8.308	8.198	8.418	0.703
	∞	8.705	8.695	8.695	8.695	0.114
1.0	0	4.917	4.918	4.918	4.918	0.020
	1	4.954	4.960	4.933	4.988	0.121
	10	5.114	5.128	5.088	5.168	0.273
	∞	5.289	5.278	5.278	5.278	0.207
1.5	0	4.126	4.128	4.128	4.128	0.048
	1	4.139	4.138	4.128	4.148	0.024
	10	4.202	4.208	4.188	4.228	0.142
	∞	4.292	4.288	4.288	4.288	0.093

476 5. Conclusion

477 In this study, a separation-of-variables dynamic stiffness matrix (SOV-
 478 DSM) method has been developed for the vibration analysis of orthotropic
 479 rectangular plates with general homogeneous boundary conditions. The

480 boundary conditions of the SOV-type plate are extended to homogeneous
481 elastically restrained boundaries beyond the classical cases, resulting in two
482 more complex eigenvalue equations. Existing SOV methods face the chal-
483 lenge of solving six unknown variables (α_1 , β_1 , Ω_x , α_2 , β_2 , Ω_y) through six
484 eigenvalue equations, which leads to high computational cost and conver-
485 gence difficulties. To address this, dynamic stiffness matrices are formulated
486 based on the SOV-type plate, and an enhanced Wittrick–Williams (W–W)
487 algorithm is introduced to solve these matrices regardless of the complexity of
488 the highly nonlinear eigenvalue equations derived from them. This enhanced
489 W–W algorithm resolves the well-known J_0 problem by providing an explicit
490 closed-form expression for the J_0 term, derived from the characteristics of
491 SOV-type plates. Furthermore, a novel yet simple numerical technique is
492 proposed for mode shape calculation, making it applicable to all boundary
493 conditions.

494 Classical boundary conditions, such as guided, simply supported, clamped,
495 and free edges, can be realized by setting the translational springs (k^v) and
496 rotational springs (k^r) along the plate edges to either zero or infinity, as ap-
497 propiate. Numerical experiments validate the high accuracy of this approach
498 for these boundary conditions. The results shows that the SOV solution can
499 also be extended to handle elastically restrained boundary conditions. De-
500 spite certain approximations inherent in few elastically restrained cases, the
501 maximum percentage error across all numerical experiments remains within
502 1.25%. This may occur because the SOV solution used is derived from the
503 weak-form governing equation, which is based on Rayleigh’s principle.

504 As a closed-form dynamic stiffness formulation, this approach has the
505 potential to construct more concise and lower-dimensional dynamic stiffness
506 matrices for orthotropic rectangular plate assemblies compared to existing
507 DSM approaches.

508 **Appendix A Integral parameters**

509 The integral parameters I_1 , I_2 , I_3 , and I_4 are defined as follows:

$$\begin{aligned}
 I_1 &= \int_0^1 \psi^2 d\eta \\
 &= (B_1^2 + B_2^2 - B_3^2 + B_4^2) + \frac{-B_1^2 + B_2^2}{2\alpha_2} \sin(2\alpha_2) + \frac{B_3^2 + B_4^2}{2\beta_2} \sinh(2\beta_2) \\
 &\quad + \frac{4(\alpha_2 B_2 B_4 + \beta_2 B_1 B_3)}{\alpha_2^2 + \beta_2^2} \sin(\alpha_2) \cosh(\beta_2) \\
 &\quad + \frac{4(-\alpha_2 B_1 B_3 + \beta_2 B_2 B_4)}{\alpha_2^2 + \beta_2^2} \cos(\alpha_2) \sinh(\beta_2).
 \end{aligned} \tag{A.1}$$

510

$$\begin{aligned}
 I_2 &= \int_0^1 \left(\psi \frac{d^2\psi}{d\eta^2} \right) d\eta \\
 &= (-\alpha_2^2 B_1^2 - \alpha_2^2 B_2^2 - \beta_2^2 B_3^2 + \beta_2^2 B_4^2) \\
 &\quad + \frac{\alpha_2(B_1^2 - B_2^2)}{2} \sin(2\alpha_2) + \frac{\beta_2(B_3^2 + B_4^2)}{2} \sinh(2\beta_2) \\
 &\quad + \frac{2(-\alpha_2^2 + \beta_2^2)(\alpha_2 B_2 B_4 + \beta_2 B_1 B_3)}{\alpha_2^2 + \beta_2^2} \sin(\alpha_2) \cosh(\beta_2) \\
 &\quad + \frac{2(-\alpha_2^2 + \beta_2^2)(-\alpha_2 B_1 B_3 + \beta_2 B_2 B_4)}{\alpha_2^2 + \beta_2^2} \cos(\alpha_2) \sinh(\beta_2).
 \end{aligned} \tag{A.2}$$

511

$$\begin{aligned}
 I_3 &= \int_0^1 \left(\frac{d\psi}{d\eta} \right)^2 d\eta \\
 &= \alpha_2^2 B_1^2 + \alpha_2^2 B_2^2 + \beta_2^2 B_3^2 - \beta_2^2 B_4^2 \\
 &\quad + \frac{\alpha_2(B_1^2 - B_2^2)}{2} \sin(2\alpha_2) + \frac{\beta_2(B_3^2 + B_4^2)}{2} \sinh(2\beta_2) \\
 &\quad + \frac{4\alpha_2\beta_2(\alpha_2 B_1 B_3 - \beta_2 B_2 B_4)}{\alpha_2^2 + \beta_2^2} \sin(\alpha_2) \cosh(\beta_2) \\
 &\quad + \frac{4\alpha_2\beta_2(\alpha_2 B_2 B_4 + \beta_2 B_1 B_3)}{\alpha_2^2 + \beta_2^2} \cos(\alpha_2) \sinh(\beta_2).
 \end{aligned} \tag{A.3}$$

512

$$\begin{aligned}
I_4 &= \int_0^1 \left(\frac{d^2\psi}{d\eta^2} \right)^2 d\eta \\
&= \left(\alpha_2^4 B_1^2 + \alpha_2^4 B_2^2 - \beta_2^4 B_3^2 + \beta_2^4 B_4^2 \right) \\
&\quad + \frac{\alpha_2^3(-B_1^2 + B_2^2)}{2} \sin(2\alpha_2) + \frac{\beta_2^3(B_3^2 + B_4^2)}{2} \sinh(2\beta_2) \\
&\quad + \frac{4\alpha_2^2\beta_2^2(-\alpha_2 B_2 B_4 - \beta_2 B_1 B_3)}{\alpha_2^2 + \beta_2^2} \sin(\alpha_2) \cosh(\beta_2) \\
&\quad + \frac{4\alpha_2^2\beta_2^2(\alpha_2 B_1 B_3 - \beta_2 B_2 B_4)}{\alpha_2^2 + \beta_2^2} \cos(\alpha_2) \sinh(\beta_2)
\end{aligned} \tag{A.4}$$

513 The integral parameters J_1 , J_2 , J_3 , and J_4 can be obtained by replacing B_1
514 to B_4 by A_1 to A_4 , respectively, and α_2 and β_2 by α_1 and β_1 , respectively.

515 **Appendix B $J(\bar{p}_1)$ count for S-G boundary conditions**

516 If the S-G boundary conditions are selected as the specific boundary con-
517 ditions to solve the $J(\bar{p}_1, \omega^*)$, then, from the eigenvalue equations in the x -
518 and y -directions,

$$\cos 2\alpha_1 = 0, \tag{B.1a}$$

$$\cos 2\alpha_2 = 0, \tag{B.1b}$$

519 the closed-form solution of the n_x -th S-G boundary conditions Ω_{x,n_x} for the
520 given n_y -order $\psi_{n_y}(\eta)$, can be expressed as

$$\begin{aligned}
b\Omega_{x,n_x}^4 &= \left[\frac{1}{\chi^2} \left(\frac{n_x \pi}{2} - \frac{\pi}{4} \right)^2 - \frac{D_{12}S_2}{D_{11}S_1} + 2\frac{D_{66}S_3}{D_{11}S_1} \right]^2 \\
&\quad - \left(\frac{D_{12}S_2}{D_{11}S_1} - 2\frac{D_{66}S_3}{D_{11}S_1} \right)^2 + \frac{D_{22}S_4}{D_{11}S_1},
\end{aligned} \tag{B.2}$$

521 and the closed-form solution of the n_y -th S-G boundary conditions frequency
 522 Ω_{y,n_y} for the given n_x -order $\phi_{n_x}(\xi)$ can be obtained as:

$$a\Omega_{y,n_y}^4 = \frac{D_{22}}{D_{11}} \left\{ \left[\chi^2 \left(\frac{n_y \pi}{2} - \frac{\pi}{4} \right)^2 - \frac{D_{12}T_2}{D_{22}T_1} + 2 \frac{D_{66}T_3}{D_{22}T_1} \right]^2 - \left(\frac{D_{12}T_2}{D_{22}T_1} - 2 \frac{D_{66}T_3}{D_{22}T_1} \right)^2 + \frac{D_{11}T_4}{D_{22}T_1} \right\}. \quad (\text{B.3})$$

523

524 References

- 525 [1] M. E. Biancolini, C. Brutti, L. Reccia, Approximate solution for free
 526 vibrations of thin orthotropic rectangular plates, Journal of Sound and
 527 Vibration 288 (1-2) (2005) 321–344. doi:10.1016/j.jsv.2005.01.005.
- 528 [2] L. Navier, Extrait des recherches sur la flexion des plans élastiques, Bull.
 529 Sci. Soc. Philomat. (1823) 95–102.
- 530 [3] M. Levy, Sur l'équilibre élastique d'une plaque rectangulaire, Comptes
 531 Rendus Acad. Sci. Paris 129 (1899) 535–539.
- 532 [4] A. W. Leissa, The free vibration of rectangular plates, Journal of Sound
 533 and Vibration 31 (3) (1973) 257–293. doi:10.1016/S0022-460X(73)
 534 80371-2.
- 535 [5] K. Y. Lam, K. C. Hung, S. T. Chow, Vibration analysis of plates with
 536 cutouts by the modified rayleigh-ritz method, Applied Acoustics 28 (1)
 537 (1989) 49–60. doi:10.1016/0003-682X(89)90030-3.
- 538 [6] S. Zhao, J. Sun, X. Ma, J. Sun, Y. An, K. Li, T. Wang, Free vibration
 539 analysis of thin rectangular plates with mixed point support conditions
 540 using the rayleigh–ritz method, Journal of Aerospace Engineering 38 (5)
 541 (2025) 04025067. doi:10.1061/JAEEZ.ASENG-6193.

- 542 [7] R. Jain, M. S. Azam, P. P. Singh, Bending analysis of functionally graded
543 plates resting on elastic foundation: A rayleigh-ritz approach and ann
544 method, *Mechanics of Advanced Materials and Structures* 31 (29) (2024)
545 11484–11502. doi:[10.1080/15376494.2024.2307474](https://doi.org/10.1080/15376494.2024.2307474).
- 546 [8] A. Bagheri, A. Mortezaei, M. A. Sayarinejad, Analysis of free in-plane vi-
547 brations of a rectangular plate with various boundary conditions canon-
548 ical form using the modified riley-ritz method, *Results in Engineering*
549 21 (2024) 101768. doi:[10.1016/j.rineng.2024.101768](https://doi.org/10.1016/j.rineng.2024.101768).
- 550 [9] P. A. Laura, B. F. Saffell Jr, Study of small-amplitude vibrations
551 of clamped rectangular plates using polynomial approximations, *The
552 Journal of the Acoustical Society of America* 41 (4A) (1967) 836–839.
553 doi:[10.1121/1.1910414](https://doi.org/10.1121/1.1910414).
- 554 [10] P. Krysl, T. Belytschko, Analysis of thin plates by the element-free
555 galerkin method, *Computational Mechanics* 17 (1) (1995) 26–35. doi:
556 [10.1007/BF00356476](https://doi.org/10.1007/BF00356476).
- 557 [11] H. Ma, J. Chen, J. Deng, Analysis of the dynamic response for kirch-
558 hoff plates by the element-free galerkin method, *Journal of Compu-
559 tational and Applied Mathematics* 451 (2024) 116093. doi:[10.1016/j.cam.2024.116093](https://doi.org/10.1016/j.cam.2024.116093).
- 561 [12] H. Ma, J. Chen, J. Deng, Error analysis of the element-free galerkin
562 method for a nonlinear plate problem, *Computers & Mathematics with
563 Applications* 163 (2024) 56–65. doi:[10.1016/j.camwa.2024.03.020](https://doi.org/10.1016/j.camwa.2024.03.020).
- 564 [13] M. S. Pereira, M. V. Donadon, Modified consistent element-free galerkin
565 method applied to reissner–mindlin plates, *Thin-Walled Structures* 212
566 (2025) 113185. doi:[10.1016/j.tws.2025.113185](https://doi.org/10.1016/j.tws.2025.113185).
- 567 [14] Y. Zhao, K. Yuan, B. Qin, L. Shen, Z. Wang, A fast polynomial-fe
568 method for the vibration of the composite laminate quadrilateral plates

- 569 and shells based on the segmentation strategy, Composite Structures
570 338 (2024) 118035. doi:10.1016/j.compstruct.2024.118035.
- 571 [15] Y. Yang, M. J. Kingan, B. R. Mace, Analysis of the forced response
572 of coupled panels using a hybrid finite element/wave and finite element
573 method, Journal of Sound and Vibration 537 (2022) 117174. doi:10.
574 1016/j.jsv.2022.117174.
- 575 [16] R. R. Paccola, M. S. M. Sampaio, H. B. Coda, Continuous stress dis-
576 tribution following transverse direction for fem orthotropic laminated
577 plates and shells, Applied Mathematical Modelling 40 (15-16) (2016)
578 7382–7409. doi:10.1016/j.apm.2016.03.005.
- 579 [17] E. Carrera, D. Scano, Finite elements based on jacobi shape functions
580 for the free vibration analysis of beams, plates, and shells, Mechanics of
581 Advanced Materials and Structures 31 (1) (2024) 4–12. doi:10.1080/
582 15376494.2023.2219438.
- 583 [18] C. Yang, J. Nakaoka, S. Hirose, Semi-analytical fem for modelling 3d
584 guided waves scattering in an infinite plate, Applied Mathematical Mod-
585 elling (2025) 116236doi:10.1016/j.apm.2025.116236.
- 586 [19] Z. Ding, Natural frequencies of rectangular plates using a set of static
587 beam functions in rayleigh-ritz method, Journal of Sound and Vibration
588 189 (1) (1996) 81–87. doi:10.1006/jsvi.1996.0006.
- 589 [20] K. Y. Cheung, D. Zhou, The free vibrations of tapered rectangular plates
590 using a new set of beam functions with the rayleigh–ritz method, Journal
591 of Sound and Vibration 223 (5) (1999) 703–722. doi:10.1006/jsvi.
592 1998.2160.
- 593 [21] Y. K. Cheung, D. Zhou, The free vibrations of rectangular compos-
594 itive plates with point-supports using static beam functions, Compos-

- 595 ite Structures 44 (2-3) (1999) 145–154. doi:10.1016/S0263-8223(98)
596 00122-6.
- 597 [22] D. Zhou, Vibrations of point-supported rectangular plates with variable
598 thickness using a set of static tapered beam functions, International
599 Journal of Mechanical Sciences 44 (1) (2002) 149–164. doi:10.1016/
600 S0020-7403(01)00081-9.
- 601 [23] R. B. Bhat, Natural frequencies of rectangular plates using character-
602 istic orthogonal polynomials in rayleigh-ritz method, Journal of Sound
603 and Vibration 102 (4) (1985) 493–499. doi:10.1016/S0022-460X(85)
604 80109-7.
- 605 [24] X. Xie, G. Jin, An efficient domain decomposition approach for the free
606 and forced vibration analysis of plate assemblies, Thin-Walled Struc-
607 tures (2025) 113621doi:10.1016/j.tws.2025.113621.
- 608 [25] Z. Celep, Z. Özcan, A. Güner, Elastic triangular plate dynamics on uni-
609 lateral winker foundation: Analysis using chebyshev polynomial ex-
610 pansion for forced vibrations, Journal of Mechanical Science and Technology
611 39 (1) (2025) 65–79. doi:10.1007/s12206-024-1207-5.
- 612 [26] N. Madinier, Q. Leclère, K. Ege, A. Berry, Spatial and frequency identi-
613 fication of the dynamic properties of thin plates with the frequency-
614 adapted virtual fields method, Journal of Sound and Vibration 596
615 (2025) 118760. doi:10.1016/j.jsv.2024.118760.
- 616 [27] X. Sun, R. Gao, Y. Zhang, Spectral stochastic isogeometric analysis of
617 bending and free vibration of porous functionally graded plates, Ap-
618 plied Mathematical Modelling 116 (2023) 711–734. doi:10.1016/j.
619 apm.2022.12.017.
- 620 [28] C. P. Filipich, M. B. Rosales, Arbitrary precision frequencies of a free

- 621 rectangular thin plate, *Journal of Sound and Vibration* 230 (3) (2000)
622 521–539. [doi:10.1006/jsvi.1999.2629](https://doi.org/10.1006/jsvi.1999.2629).
- 623 [29] Y. V. S. Kumar, J. K. Paik, Buckling analysis of cracked plates using hi-
624 erarchical trigonometric functions, *Thin-Walled Structures* 42 (5) (2004)
625 687–700. [doi:10.1016/j.tws.2003.12.012](https://doi.org/10.1016/j.tws.2003.12.012).
- 626 [30] G. A. Yessenbayeva, F. M. Akhanov, T. K. Makazhanova, On the cal-
627 culation of rectangular plates by the trigonometric series, *Bulletin of
628 the Karaganda University. Mathematics Series* 94 (2) (2019) 115–120.
629 [doi:10.31489/2019M2/115-120](https://doi.org/10.31489/2019M2/115-120).
- 630 [31] G. He, D. Cao, J. Wei, Y. Cao, Z. Chen, Study on analytical global
631 modes for a multi-panel structure connected with flexible hinges, *Ap-
632 plied Mathematical Modelling* 91 (2021) 1081–1099. [doi:10.1016/j.apm.2020.10.044](https://doi.org/10.1016/j.apm.2020.10.044).
- 633 [32] J. Su, W. He, K. Zhang, Q. Zhang, Y. Qu, Vibration analysis of func-
634 tionally graded porous cylindrical shells filled with dense fluid using an
635 energy method, *Applied Mathematical Modelling* 108 (2022) 167–188.
636 [doi:10.1016/j.apm.2022.03.028](https://doi.org/10.1016/j.apm.2022.03.028).
- 637 [33] W. L. Li, Vibration analysis of rectangular plates with general elastic
638 boundary supports, *Journal of Sound and Vibration* 273 (3) (2004) 619–
639 635. [doi:10.1016/S0022-460X\(03\)00562-5](https://doi.org/10.1016/S0022-460X(03)00562-5).
- 640 [34] Y. K. Cheung, D. Zhou, Vibrations of moderately thick rectangular
641 plates in terms of a set of static timoshenko beam functions, *Computers
642 & Structures* 78 (6) (2000) 757–768. [doi:10.1016/S0045-7949\(00\)00058-4](https://doi.org/10.1016/S0045-7949(00)
643 00058-4).
- 644 [35] D. Zhou, Vibrations of mindlin rectangular plates with elastically re-
645 strained edges using static timoshenko beam functions with the rayleigh–
646

- ritz method, International Journal of Solids and Structures 38 (32-33) (2001) 5565–5580. doi:10.1016/S0020-7683(00)00384-X.
- [36] L. E. Monterrubio, S. Ilanko, Proof of convergence for a set of admissible functions for the rayleigh–ritz analysis of beams and plates and shells of rectangular planform, Computers & Structures 147 (2015) 236–243. doi:10.1016/j.compstruc.2014.09.008.
- [37] F. C. Onyeka, B. O. Mama, C. D. Nwa-David, Application of variation method in three dimensional stability analysis of rectangular plate using various exact shape functions, Nigerian Journal of Technology 41 (1) (2022) 8–20. doi:10.4314/njt.v41i1.2.
- [38] L. V. Kantorovich, V. I. Krylov, Approximate Methods of Higher Analysis, Interscience Publishers, New York, 1958.
- [39] A. D. Kerr, An extension of the kantorovich method, Quarterly of Applied Mathematics 26 (2) (1968) 219–229. doi:10.1090/qam/99857.
- [40] A. D. Kerr, H. Alexander, An application of the extended kantorovich method to the stress analysis of a clamped rectangular plate, Acta Mechanica 6 (2) (1968) 180–196. doi:10.1007/BF01170382.
- [41] H. Rostami, A. R. Ranji, F. Bakhtiari-Nejad, Free in-plane vibration analysis of rotating rectangular orthotropic cantilever plates, International Journal of Mechanical Sciences 115 (2016) 438–456. doi:10.1016/j.ijmecsci.2016.07.030.
- [42] B. Huang, H. S. Kim, Interlaminar stress analysis of piezo-bonded composite laminates using the extended kantorovich method, International Journal of Mechanical Sciences 90 (2015) 16–24. doi:10.1016/j.ijmecsci.2014.11.003.
- [43] I. Shufrin, M. Eisenberger, Semi-analytical modeling of cutouts in rectangular plates with variable thickness–free vibration analysis, Applied

- 674 Mathematical Modelling 40 (15-16) (2016) 6983–7000. doi:10.1016/j.apm.2016.02.020.
- 675
- 676 [44] A. Singh, P. Kumari, Three-dimensional free vibration analysis of com-
677 posite fgm rectangular plates with in-plane heterogeneity: An ekm so-
678 lution, International Journal of Mechanical Sciences 180 (2020) 105711.
679 doi:10.1016/j.ijmecsci.2020.105711.
- 680 [45] W.-X. Zhong, A new systematic methodology for theory of elasticity,
681 Dalian University of Technology Press, Dalian (1995) 182–187.
- 682 [46] Y. Xing, B. Liu, New exact solutions for free vibrations of rectangular
683 thin plates by symplectic dual method, Acta Mechanica Sinica 25 (2009)
684 265–270. doi:10.1007/s10409-008-0208-4.
- 685 [47] C. W. Lim, C. F. Lü, Y. Xiang, W. Yao, On new symplectic elastic-
686 ity approach for exact free vibration solutions of rectangular kirchhoff
687 plates, International Journal of Engineering Science 47 (1) (2009) 131–
688 140. doi:10.1016/j.ijengsci.2008.08.003.
- 689 [48] Y. Shi, D. An, Z. Wu, L. Liang, L. Chen, R. Li, Symplectic analytical
690 solutions for free vibration of elastically line-hinged orthotropic rectan-
691 gular plates with rotationally restrained edges, Applied Mathematical
692 Modelling 136 (2024) 115629. doi:10.1016/j.apm.2024.08.001.
- 693 [49] D. Xu, J. Xu, S. Xiong, L. Chen, Q. He, B. Wang, R. Li, Hamiltonian
694 system-based analytic thermal buckling solutions of orthotropic rectan-
695 gular plates, International Journal of Mechanical Sciences 267 (2024)
696 108987. doi:10.1016/j.ijmecsci.2024.108987.
- 697 [50] Y. Shi, D. An, Z. Hu, Z. Zhou, R. Li, Free vibration solutions of rota-
698 tionally restrained stepped thick rectangular plates utilizing a symplec-
699 tic analytical framework, Applied Mathematical Modelling 143 (2025)
700 116044. doi:10.1016/j.apm.2025.116044.

- 701 [51] Y. F. Xing, B. Liu, New exact solutions for free vibrations of thin or-
702 thotropic rectangular plates, Composite Structures 89 (4) (2009) 567–
703 574. doi:[10.1016/j.compstruct.2008.11.010](https://doi.org/10.1016/j.compstruct.2008.11.010).
- 704 [52] Y. Xing, Q. Sun, B. Liu, Z. Wang, The overall assessment of closed-
705 form solution methods for free vibrations of rectangular thin plates,
706 International Journal of Mechanical Sciences 140 (2018) 455–470. doi:
707 [10.1016/j.ijmecsci.2018.03.013](https://doi.org/10.1016/j.ijmecsci.2018.03.013).
- 708 [53] Y. Xing, Z. Wang, An extended separation-of-variable method for
709 the free vibration of orthotropic rectangular thin plates, International
710 Journal of Mechanical Sciences 182 (2020) 105739. doi:[10.1016/j.ijmecsci.2020.105739](https://doi.org/10.1016/j.ijmecsci.2020.105739).
- 712 [54] Y. Xing, Z. Wang, An improved separation-of-variable method for the
713 free vibration of orthotropic rectangular thin plates, Composite Struc-
714 tures 252 (2020) 112664. doi:[10.1016/j.compstruct.2020.112664](https://doi.org/10.1016/j.compstruct.2020.112664).
- 715 [55] Y. Xing, G. Li, Y. Yuan, A review of the analytical solution methods
716 for the eigenvalue problems of rectangular plates, International Journal
717 of Mechanical Sciences 221 (2022) 107171. doi:[10.1016/j.ijmecsci.2022.107171](https://doi.org/10.1016/j.ijmecsci.2022.107171).
- 719 [56] Z. Wang, Y. Xing, G. Li, Closed-form solutions for the free vibrations of
720 three-dimensional orthotropic rectangular plates, International Journal
721 of Mechanical Sciences 199 (2021) 106398. doi:[10.1016/j.ijmecsci.2021.106398](https://doi.org/10.1016/j.ijmecsci.2021.106398).
- 723 [57] Z. Wang, Y. Xing, An extended separation-of-variable method for free
724 vibrations of orthotropic rectangular thin plate assemblies, Thin-Walled
725 Structures 169 (2021) 108491. doi:[10.1016/j.tws.2021.108491](https://doi.org/10.1016/j.tws.2021.108491).
- 726 [58] Z. Wang, Y. Xing, Q. Sun, Y. Yang, Highly accurate closed-
727 form solutions for free vibration and eigenbuckling of rectangular

- 728 nanoplates, Composite Structures 210 (2019) 822–830. doi:10.1016/
729 j.compstruct.2018.11.094.
- 730 [59] Z. Wang, Y. Xing, Q. Sun, Highly accurate closed-form solutions for the
731 free in-plane vibration of rectangular plates with arbitrary homogeneous
732 boundary conditions, Journal of Sound and Vibration 470 (2020) 115166.
733 doi:10.1016/j.jsv.2019.115166.
- 734 [60] J. R. Banerjee, Dynamic stiffness formulation for structural elements:
735 a general approach, Computers & Structures 63 (1997) 101–103. doi:
736 10.1016/S0045-7949(96)00326-4.
- 737 [61] S. O. Papkov, J. R. Banerjee, Dynamic stiffness formulation and free
738 vibration analysis of specially orthotropic mindlin plates with arbitrary
739 boundary conditions, Journal of Sound and Vibration 458 (2019) 522–
740 543. doi:10.1016/j.jsv.2019.06.028.
- 741 [62] X. Liu, S. Tao, X. Zhao, X. Liu, Z. Lu, F. Liu, Dynamic response analysis
742 for bridges subjected to moving vehicle loads by using the analytical
743 dynamic stiffness method, Computers & Structures 292 (2024) 107240.
744 doi:10.1016/j.compstruc.2023.107240.
- 745 [63] M. Boscolo, J. Banerjee, Dynamic stiffness elements and their applica-
746 tions for plates using first order shear deformation theory, Computers &
747 Structures 89 (3-4) (2011) 395–410. doi:10.1016/j.compstruc.2010.
748 11.005.
- 749 [64] F. Fazzolari, M. Boscolo, J. Banerjee, An exact dynamic stiffness ele-
750 ment using a higher order shear deformation theory for free vibration
751 analysis of composite plate assemblies, Composite Structures 96 (2013)
752 262–278. doi:10.1016/j.compstruct.2012.08.033.
- 753 [65] O. Ghorbel, J.-B. Casimir, L. Hammami, I. Tawfiq, M. Haddar, Dy-

- 754 namic stiffness formulation for free orthotropic plates, Journal of Sound
755 and Vibration 346 (2015) 361–375. doi:10.1016/j.jsv.2015.02.020.
- 756 [66] F. W. Williams, H. J. Ouyang, D. Kennedy, C. B. York, Wave propa-
757 gation along longitudinally periodically supported or stiffened prismatic
758 plate assemblies, Journal of Sound and Vibration 186 (2) (1995) 197–
759 205. doi:10.1006/jsvi.1995.0443.
- 760 [67] J. Banerjee, S. Papkov, X. Liu, D. Kennedy, Dynamic stiffness matrix of
761 a rectangular plate for the general case, Journal of Sound and Vibration
762 342 (2015) 177–199. doi:10.1016/j.jsv.2014.12.031.
- 763 [68] X. Liu, J. Banerjee, Free vibration analysis for plates with arbi-
764 trary boundary conditions using a novel spectral-dynamic stiffness
765 method, Computers & Structures 164 (2016) 108–126. doi:10.1016/j.
766 compstruc.2015.11.005.
- 767 [69] X. Liu, W. Zhou, M. Filippi, Y. Wang, A wavenumber dynamic stiff-
768 ness method for exact and efficient dispersion analysis of plate built-
769 up waveguides, Journal of Sound and Vibration 591 (2024) 118605.
770 doi:10.1016/j.jsv.2024.118605.
- 771 [70] W. Zhou, X. Liu, Y. Wang, X. Zhao, Wavenumber dynamic stiffness
772 formulation for exact dispersion analysis of moderately thick symmetric
773 cross-ply laminated plate built-up waveguides, Thin-Walled Structures
774 204 (2024) 112305. doi:10.1016/j.tws.2024.112305.
- 775 [71] X. Liu, J. Banerjee, An exact spectral-dynamic stiffness method for free
776 flexural vibration analysis of orthotropic composite plate assemblies—
777 part i: Theory, Composite Structures 132 (2015) 1274–1287. doi:10.
778 1016/j.comstruct.2015.07.020.
- 779 [72] S. Timoshenko, Theory of Plates and Shells, McGraw-Hill Book Com-
780 pany, 1940.

- 781 [73] D. J. Gorman, Free in-plane vibration analysis of rectangular plates
782 with elastic support normal to the boundaries, *Journal of Sound and*
783 *Vibration* 285 (4-5) (2005) 941–966. doi:10.1016/j.jsv.2004.09.017.
- 784 [74] Y. Mochida, S. Ilanko, Transient vibration analysis of a completely free
785 plate using modes obtained by gorman’s superposition method, *Journal*
786 *of Sound and Vibration* 329 (10) (2010) 1890–1900. doi:10.1016/j.
787 j.jsv.2009.11.029.
- 788 [75] B. Wang, P. Li, R. Li, Symplectic superposition method for new analytic
789 buckling solutions of rectangular thin plates, *International Journal of*
790 *Mechanical Sciences* 119 (2016) 432–441. doi:10.1016/j.ijmecsci.
791 2016.11.006.
- 792 [76] Z. Hu, X. Zheng, D. An, C. Zhou, Y. Yang, R. Li, New analytic buck-
793 ling solutions of side-cracked rectangular thin plates by the symplectic
794 superposition method, *International Journal of Mechanical Sciences* 191
795 (2021) 106051. doi:10.1016/j.ijmecsci.2020.106051.
- 796 [77] Z. Wang, D. Xu, J. Li, Z. Hu, G. Gong, R. Li, New analytical buck-
797 ling solutions for non-lévy-type graphene-reinforced composite lami-
798 nated plates, *Composite Structures* 360 (2025) 119067. doi:10.1016/
799 j.compstruct.2025.119067.
- 800 [78] H. Khov, W. L. Li, R. F. Gibson, An accurate solution method for
801 the static and dynamic deflections of orthotropic plates with general
802 boundary conditions, *Composite Structures* 90 (4) (2009) 474–481. doi:
803 10.1016/j.compstruct.2009.04.020.
- 804 [79] W. L. Li, X. Zhang, J. Du, Z. Liu, An exact series solution for the
805 transverse vibration of rectangular plates with general elastic boundary
806 supports, *Journal of Sound and Vibration* 321 (1-2) (2009) 254–269.
807 doi:10.1016/j.jsv.2008.09.035.

- 808 [80] Y. M. Grigorenko, L. S. Rozhok, Discrete fourier-series method in
809 problems of bending of variable-thickness rectangular plates, Journal
810 of Engineering Mathematics 46 (3) (2003) 269–280. doi:10.1023/A:
811 1025076708442.
- 812 [81] Q. Wang, D. Shi, Q. Liang, F. Ahad, An improved fourier series solution
813 for the dynamic analysis of laminated composite annular, circular, and
814 sector plate with general boundary conditions, Journal of Composite
815 Materials 50 (30) (2016) 4199–4233. doi:10.1177/00219983166352.
- 816 [82] B. Leng, S. Ullah, T. Yu, K. Li, New analytical free vibration solutions
817 of thin plates using the fourier series method, Applied Sciences 12 (17)
818 (2022) 8631. doi:10.3390/app12178631.
- 819 [83] R. Li, Y. Zhong, B. Tian, Y. Liu, On the finite integral transform method
820 for exact bending solutions of fully clamped orthotropic rectangular thin
821 plates, Applied Mathematics Letters 22 (12) (2009) 1821–1827. doi:
822 10.1016/j.aml.2009.07.003.
- 823 [84] Y. Zhong, X.-F. Zhao, R. Li, Free vibration analysis of rectangular can-
824 tilever plates by finite integral transform method, International Journal
825 for Computational Methods in Engineering Science and Mechanics 14 (3)
826 (2013) 221–226. doi:10.1080/15502287.2012.711424.
- 827 [85] B. Tian, R. Li, Y. Zhong, Integral transform solutions to the bend-
828 ing problems of moderately thick rectangular plates with all edges free
829 resting on elastic foundations, Applied Mathematical Modelling 39 (1)
830 (2015) 128–136. doi:10.1016/j.apm.2014.05.012.
- 831 [86] S. Zhang, L. Xu, Bending of rectangular orthotropic thin plates with ro-
832 tationally restrained edges: a finite integral transform solution, Applied
833 Mathematical Modelling 46 (2017) 48–62. doi:10.1016/j.apm.2017.
834 01.053.

- 835 [87] Y. Chen, D. An, C. Zhou, Y. Li, J. Xu, R. Li, Analytical free vibration
836 solutions of rectangular edge-cracked plates by the finite integral trans-
837 form method, International Journal of Mechanical Sciences 243 (2023)
838 108032. doi:10.1016/j.ijmecsci.2022.108032.
- 839 [88] B. Li, H. Liu, J. Liu, M. Cui, X. Gao, J. Lv, A novel weak-form mesh-
840 less method based on lagrange interpolation for mechanical analysis of
841 complex thin plates, Engineering Analysis with Boundary Elements 169
842 (2024) 106021. doi:10.1016/j.enganabound.2024.106021.
- 843 [89] Z. Zhu, Y. Song, Y. Zhang, Q. Liu, G. Wang, Sound radiation of the
844 plate with arbitrary holes, International Journal of Mechanical Sciences
845 264 (2024) 108814. doi:10.1016/j.ijmecsci.2023.108814.
- 846 [90] D. Shao, B. Li, Analytic vibration solutions for moving-loaded compos-
847 itive plates beyond lévy boundaries, International Journal of Mechanical
848 Sciences (2025) 110547doi:10.1016/j.ijmecsci.2025.110547.
- 849 [91] W. H. Wittrick, F. W. Williams, A general algorithm for comput-
850 ing natural frequencies of elastic structures, The Quarterly Journal
851 of Mechanics and Applied Mathematics 24 (3) (1971) 263–284. doi:
852 10.1093/qjmmam/24.3.263.
- 853 [92] F. Han, D. Dan, W. Cheng, J. Zang, An improved wittrick-williams
854 algorithm for beam-type structures, Composite Structures 204 (2018)
855 560–566. doi:10.1016/j.compstruct.2018.07.108.
- 856 [93] X. Liu, L. Chang, J. R. Banerjee, H.-C. Dan, Closed-form dynamic
857 stiffness formulation for exact modal analysis of tapered and functionally
858 graded beams and their assemblies, International Journal of Mechanical
859 Sciences 214 (2022) 106887. doi:10.1016/j.ijmecsci.2021.106887.
- 860 [94] S. Yuan, K. Ye, F. Williams, Second order mode-finding method in dy-

- 861 namic stiffness matrix methods, Journal of Sound and Vibration 269 (3-
862 5) (2004) 689–708. doi:10.1016/S0022-460X(03)00126-3.
- 863 [95] S. Zhang, L. Xu, R. Li, New exact series solutions for transverse vibra-
864 tion of rotationally-restrained orthotropic plates, Applied Mathematical
865 Modelling 65 (2019) 348–360. doi:10.1016/j.apm.2018.08.033.
- 866 [96] M. Mukhopadhyay, Free vibration of rectangular plates with edges hav-
867 ing different degrees of rotational restraint, Journal of Sound and Vi-
868 bration 67 (4) (1979) 459–468. doi:10.1016/0022-460X(79)90438-3.